International Journal of Earth Sciences (2024) 113:555–581
https://doi.org/10.1007/s00531-024-02389-8

ORIGINAL PAPER

Is the Yermak Plateau a continental fragment from North America? Constraints from Cretaceous and early Eocene magmatic events

Solveig Estrada[1,4] · Nikola Koglin[1] · Florian Riefstahl[2] · Hannah Nopper[2] · Wolfram Geissler[3] · Cornelia Spiegel[2]

Received: 12 July 2023 / Accepted: 16 January 2024 / Published online: 15 April 2024
© The Author(s) 2024

Abstract

The Yermak Plateau (YP) north of Svalbard is a prominent bathymetric feature in the Eurasia Basin of the Arctic Ocean, forming the northwesternmost margin of the Eurasian plate. Seismic data indicate that the YP comprises continental basement; however, little is known about its geology. New petrographic, geochemical, Sr–Nd isotopic, and Ar–Ar geochronological data were obtained on rock fragments, which were previously recovered from basement highs of the northeastern and southwestern YP and are dominantly of magmatic origin. These new data combined with available literature data, and comparisons with volcanic and sedimentary rocks from onshore and offshore areas adjacent to the YP indicate that the northeastern YP and the southwestern YP are different regarding their geological evolution. The southwestern YP comprises an alkaline basaltic suite for which an Ar–Ar biotite age of 51 Ma was previously reported. The suite was formed in a continental extensional regime offshore northern Svalbard. Associated sedimentary rocks (sandstone, several limestones) show petrographic similarity with rocks of the Devonian Old Red Sandstone on Svalbard. From the northeastern YP, in contrast, we recovered mildly alkaline basaltic rocks with mid-Cretaceous Ar–Ar ages (102 ± 3 and 98 ± 3 Ma). The rocks show certain geochemical characteristics (partial enrichments of P, Ba, and Eu), which overlap with similar-aged Cretaceous basaltic rocks from northern Ellesmere Island of Canada and North Greenland. We suggest that the northeastern YP is a continental fragment derived from the North American plate, which was separated from the conjugate Morris Jesup Rise and juxtaposed to the geologically distinct southwestern YP by the propagation of the Gakkel Ridge spreading center since the early Oligocene.

Keywords Yermak Plateau · Ar–Ar dating · HALIP · Alkaline magmatism · Morris Jesup Rise · Alpha–Mendeleev Ridge

Introduction

The submarine Yermak Plateau (YP) north of Svalbard is a prominent bathymetric feature of the Eurasia Basin at a water depth of about 500 to 1000 m (Fig. 1). It is situated at the northwesternmost margin of the Eurasian Plate near two active, ultra-slow spreading ridges, the Gakkel Ridge in the north and the Lena Trough, the central part of the Fram Strait, in the west. The boomerang-shaped YP is divided into the NNW–SSE trending part south of 82° N bordered by the Lena Trough, hereinafter referred to as southwestern YP, and the SW–NE trending part north of 82° N adjacent to the Gakkel Ridge, hereinafter referred to as northeastern YP (Fig. 2).

Our knowledge of the structure of the still mostly sea-ice covered YP results mainly from geophysical studies, comprising seismic, gravity, magnetic, and heat flow measurements (e.g., Feden et al. 1979; Crane et al. 1982; Jackson et al. 1984; Okay and Crane 1993; Jokat et al. 1995, 2008; Brozena et al. 2003; Ritzmann and Jokat 2003; Geissler et al. 2011; Berglar et al. 2016). High-amplitude positive magnetic anomalies of the northeastern YP (Fig. 2) and the conjugate Morris Jesup Rise have been interpreted as a volcanic center ("Yermak hotspot") formed during the breakup of these plateaus at about 35 Ma (Feden et al. 1979). Based on seismic

✉ Nikola Koglin
Nikola.Koglin@bgr.de

1 Bundesanstalt für Geowissenschaften und Rohstoffe, Hannover, Germany

2 Department 5 Geosciences, University of Bremen, Bremen, Germany

3 Alfred Wegener Institute Helmholtz-Centre for Polar and Marine Research, Bremerhaven, Germany

4 Present Address: Hannover, Germany

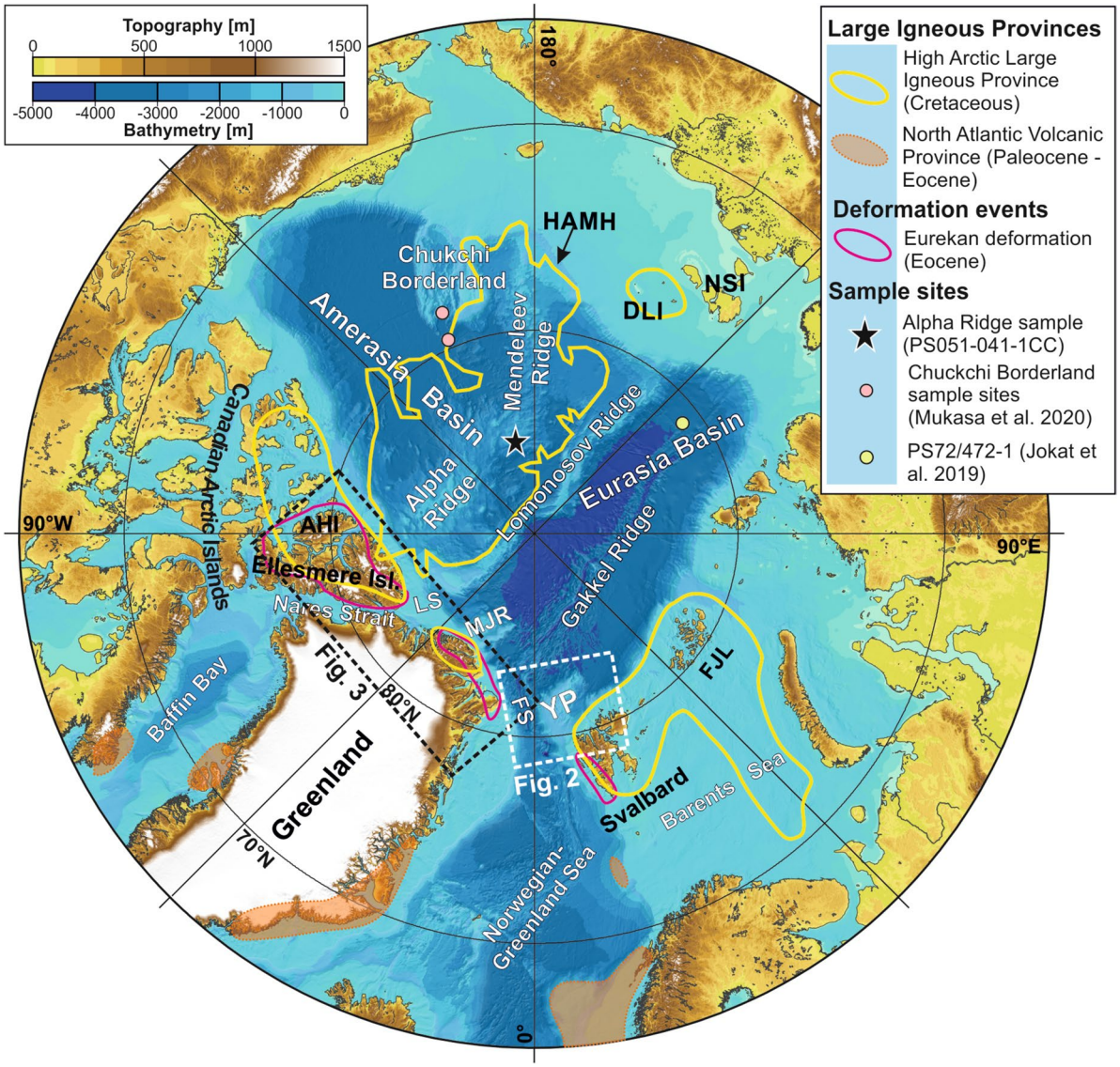

Fig. 1 Bathymetric overview map of the Arctic Ocean and surrounding continental areas based on the International Bathymetric Chart of the Arctic Ocean (IBCAO; Jakobsson et al. 2020) showing the position of our study area, the Yermak Plateau (white dashed outline). See Fig. 2 for details. The extent of large magmatic provinces, the Cretaceous High Arctic Large Igneous Province including the High Arctic Magnetic High Domain (encircled in yellow), and the Paleocene–Eocene North Atlantic Volcanic Province (translucent orange covered areas) are compiled from the literature (Storey et al. 1998, 2007; Drachev and Saunders 2006; Buchan and Ernst 2006; Tegner et al. 2008, 2011; Shipilov and Karyakin 2011; Senger et al. 2014; Shipilov 2015; Estrada et al. 2016; Oakey and Saltus 2016; Polteau et al. 2016). The areas affected by the Eurekan deformation (encircled in pink) are based on Piepjohn et al. (2016). The positions of offshore rock sampling sites referred to in this study are indicated as shown in the legend. The area enclosed by the black dashed outline is shown in detail as Fig. 3. *AHI* Axel Heiberg Island, *DLI* DeLong Islands, *FJL* Franz Josef Land, *FS* Fram Strait, *HAMH* High Arctic Magnetic High Domain, *LS* Lincoln Sea, *MJR* Morris Jesup Rise, *NSI* New Siberian Islands, *YP* Yermak Plateau

velocity data, the northeastern YP has been interpreted to be of oceanic crust and the southwestern YP to be thinned continental crust (Jackson et al. 1984). More recently, the basement of the entire YP is interpreted to consist of stretched continental crust characterized by magmatic intrusions (Ritzmann and Jokat 2003; Jokat et al. 2008, 2016; Berglar et al. 2016).

Rock samples from the acoustic basement of the YP, which can verify the geophysical models, are rare (Fig. 2). A single gneiss sample dredged from the southwestern YP (Fig. 2) was interpreted as an equivalent of the basement of northern Svalbard (Jackson et al. 1984). During the expedition ARK-XX/3 of the German RV Polarstern in 2004, several rock samples were obtained (Stein 2005) and studied

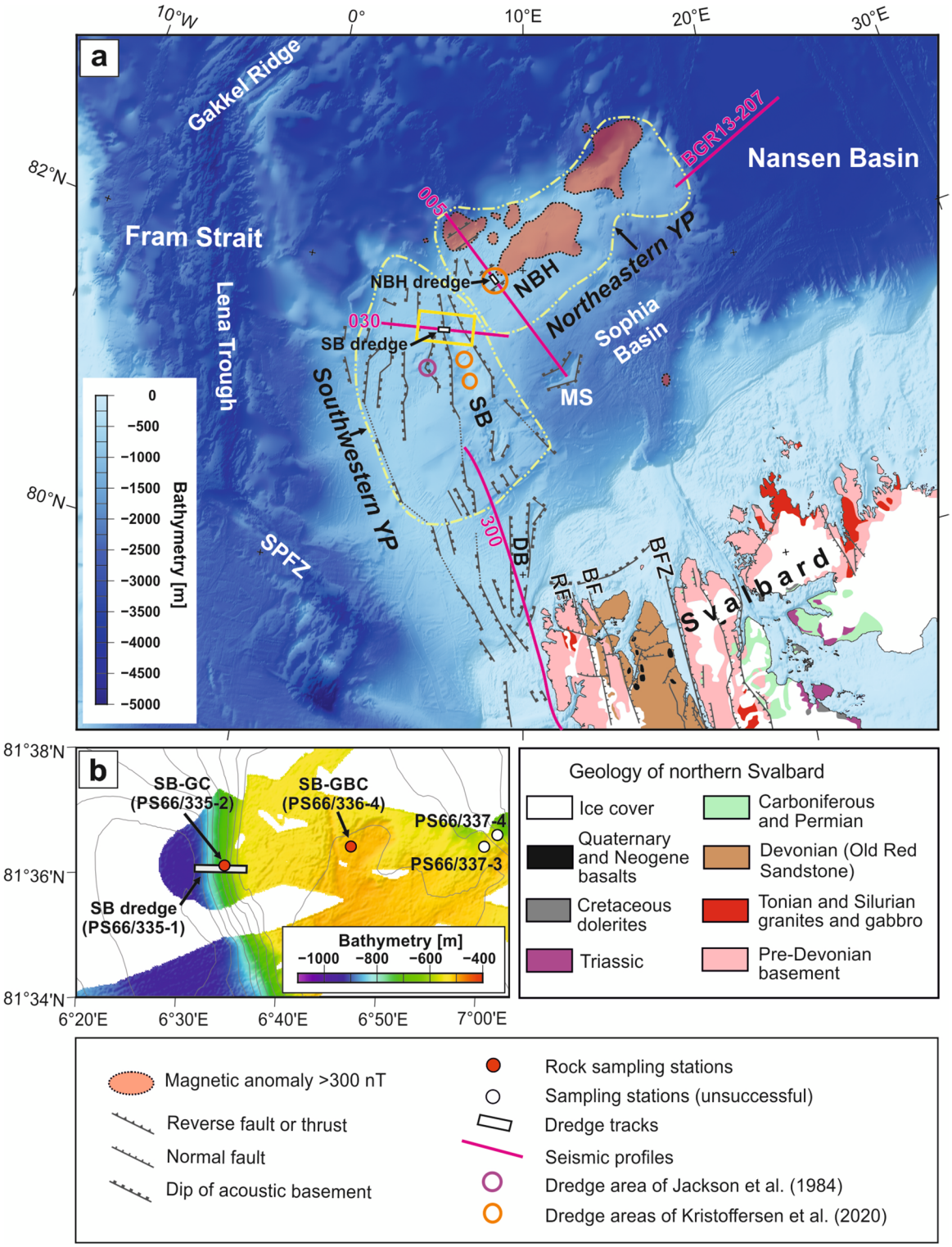

Fig. 2 **a** Bathymetric map of the YP based on the IBCAO v4 dataset (Jakobsson et al. 2020) including onshore geology of northern Svalbard (Dallmann et al. 2002) and offshore geophysical observations (dip of acoustic basement and magnetic anomaly > 300 nT; Jokat et al. 2008). The location of seismic profile lines (AWI-200400005, AWI-20040030, AWI-99300, abbreviated to the last three numbers), the NBH and SB dredge positions, and the dredge locations of Jackson et al. (1984) and Kristoffersen et al. (2020) are shown. The yellow frame shows the location of **b**. **b** Detailed bathymetric map of the northern Sverdrup Bank with the positions of the basement rock sampling stations SB-GC and SB-GBC as well as two unsuccessful stations, based on the multibeam echosounder system onboard RV Polarstern (Stein 2005). *BF* Breibogen Fault, *BFZ* Billefjorden Fault Zone, *DB* Danskøya Basin, *GBC* Giant box corer, *GC* Gravity corer, *MS* Mosby Seamount, *NBH* northern basement highs, *RF* Raudfjorden Fault, *SB* Sverdrup Bank, *SPFZ* Spitsbergen Fracture Zone

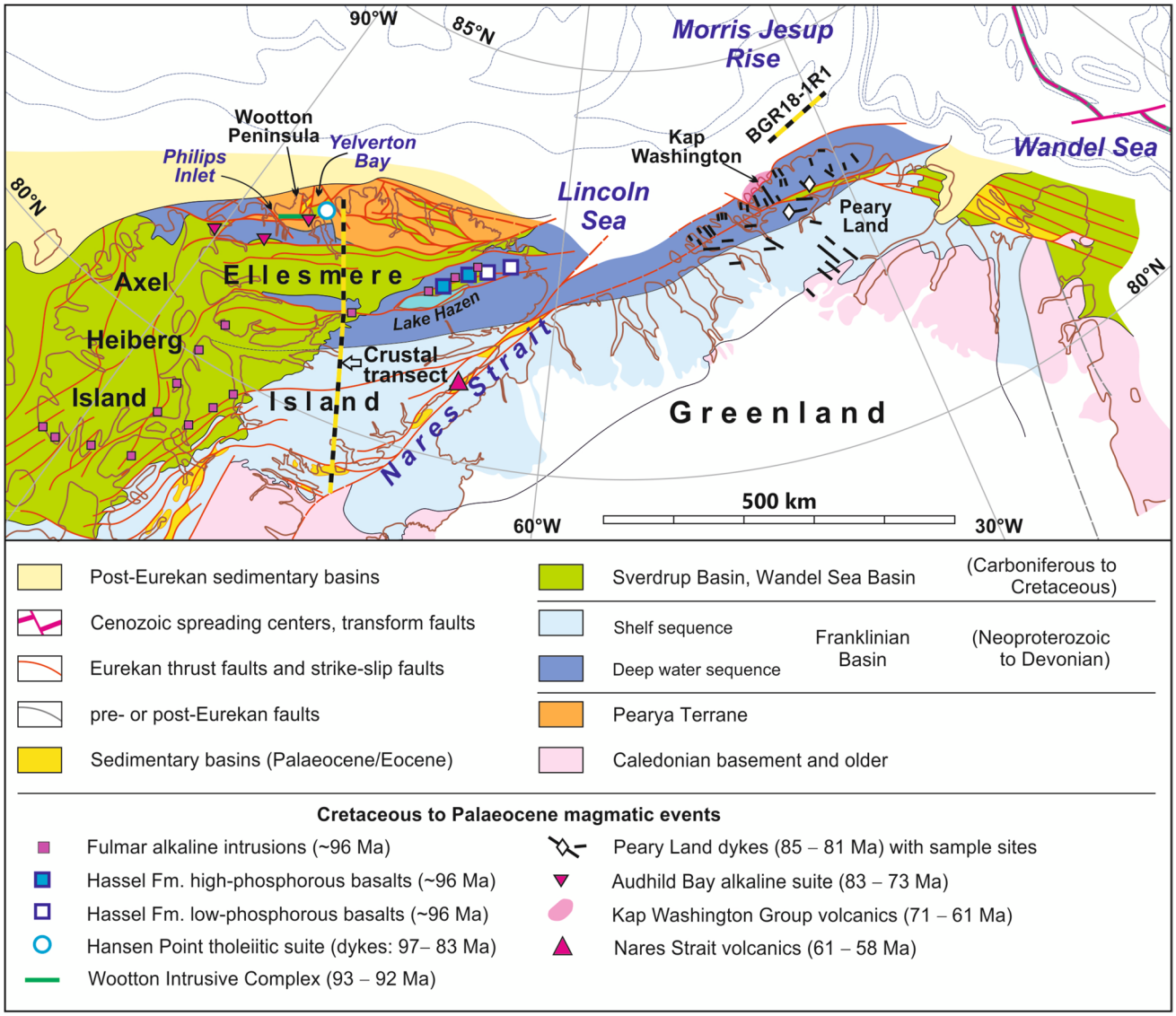

Fig. 3 Geological overview map of the northeastern Canadian Arctic and North Greenland (modified from Piepjohn et al. 2016). The locations of Cretaceous to Paleocene magmatic events referred to in this study as well as the seismic refraction line BGR18-1R1 off North Greenland (Brotzer et al. 2022) and the N–S trending crustal transect through Ellesmere Island compiled from deep seismological data (Schiffer and Stephenson 2017) are shown (black-yellow lines)

for their petrography, geochemistry, and geochronology by Riefstahl et al. (2013). More recently, rock samples have been dredged from the southwestern and northeastern parts of the plateau (Kristoffersen and Hall 2014; Kristoffersen et al. 2020). Traditionally, the geological evolution of the southwestern and northeastern parts of the YP was believed to be closely related to Svalbard, based on lithological similarities and the results of, e.g., velocity modeling (Ritzmann and Jokat 2003; Riefstahl et al. 2013; Kristoffersen et al. 2020).

Here, we present new data, which suggest a different evolution of the northeastern YP as compared to the southwestern YP. Our study is based on mineralogical and whole rock geochemical analyses, Ar–Ar dating as well as Rb–Sr and Sm–Nd isotope analyses of dredged and cored rocks, mainly of magmatic origin. Igneous rocks are most likely an important component of the basement of the YP, as is also indicated by the magnetic anomalies of the northeastern YP. With this new data, we characterize two in situ alkali basaltic suites from the northeastern and southwestern YP, which differ in age, geochemical signatures, and associated non-magmatic rocks. We compare these alkali basaltic suites with offshore and onshore basaltic rocks in the Arctic realm, including a sample from the Alpha Ridge (Fig. 1). These results allow a new plate-tectonic interpretation of the acoustic basement of the YP.

Geological setting

The Amerasia Basin and the HALIP

The Arctic Ocean comprises the Mesozoic Amerasia Basin and the Cenozoic Eurasia Basin, which are separated by a sliver of continental crust, the Lomonosov Ridge (Fig. 1). Prior to the opening of the Eurasia Basin, the YP and the conjugate Morris Jesup Rise (including Morris Jesup Spur) were part of a contiguous continental land mass at the passive margin of the Amerasia Basin (Glebovsky et al. 2006). The multistage opening of the Amerasia Basin since the Early Cretaceous was accompanied by intense, dominantly mafic igneous activity referred to as the High Arctic Large Igneous Province (HALIP) (e.g., Buchan and Ernst 2006, 2018, and references therein). The HALIP includes continental flood basalts, sills and dykes emplaced in the Barents Shelf region (Svalbard, Franz Josef Land), the De Long Islands, the Canadian Arctic islands, and North Greenland (Fig. 1). HALIP-related magmatism took place between ca. 135 and 75 Ma, with major pulses at ca. 128–120 Ma, ca. 100–92 Ma, and around 84–78 Ma (Buchan and Ernst 2018 and references therein). The flood basalt magmatism on Franz Josef Land started already in the Early Jurassic, followed by Late Jurassic to Early Cretaceous episodes peaking at around 157, 132, and 115 Ma, supported by biostratigraphic investigations (Karyakin et al. 2021; Karyakin and Aleksandrova 2022). The first magmatic pulses were tholeiitic, whereas transitional to alkaline magmatism became more important after ca. 100 Ma in the Canadian Arctic and was dominant in North Greenland (e.g., Estrada and Henjes-Kunst 2004; Tegner et al. 2011; Senger et al. 2014; Estrada 2015; Estrada et al. 2016; Buchan and Ernst 2018; Naber et al. 2021; Bédard et al. 2021a, b). The large High Arctic Magnetic High (HAMH) that covers the submarine Alpha–Mendeleev Ridge as well as neighboring areas shows magnetic patterns typical for plume-related global Large Igneous Provinces and is interpreted as part of the HALIP (Saltus et al. 2011; Oakey and Saltus 2016). However, the age of igneous rocks from the Alpha–Mendeleev Ridge is widely unknown. Basement samples dredged from the central Alpha Ridge comprise highly altered pyroclastic rocks, which show alkaline basaltic and within-plate signatures, but are undated (Van Wagoner and Robinson 1985; Van Wagoner et al. 1986). The first dated basalt sample from the central Alpha–Mendeleev Ridge, a tholeiitic basalt, yielded an Ar–Ar age on plagioclase of 89 ± 1 Ma (Jokat 1999; Jokat et al. 1999, 2013). Previously unpublished geochemical data of this basalt sample (Mühe and Jokat 2004) are used for comparison to our own data. An Ar–Ar age of 90 Ma was obtained on alkaline basaltic tuff dredged from the Alpha Ridge (Williamson et al. 2019).

A new plate-tectonic configuration in the Arctic developed since the Late Cretaceous, starting with the onset of seafloor spreading in the Labrador Sea and rifting in the Baffin Bay, as well as contemporaneous rifting in the Norwegian-Greenland Sea and the future Eurasia Basin (Kristoffersen and Talwani 1977; Srivastava 1978; Vogt et al. 1979; Gerlings et al. 2009 and references therein). An expression of these extensional processes is probably the latest stage of alkaline HALIP-related magmatism with the mafic Peary Land dykes in North Greenland, emplaced between ca. 85 and 81 Ma (Kontak et al. 2001; Thórarinsson et al. 2015), followed by the bimodal, alkaline volcanism of the Kap Washington Group at ca. 71–61 Ma (Tegner et al. 2011; Thórarinsson et al. 2011) (Fig. 3).

The Eurasia Basin and Eurekan deformation events

In the earliest Eocene, rifting turned into seafloor spreading in the Eurasia Basin, Baffin Bay, and the Norwegian–Greenland Sea (Talwani and Eldholm 1977; Vogt

Table 1 Lithology of dredge and core samples from the Yermak Plateau

	Southwestern YP, Northern Sverdrup Bank			Northeastern YP
	SB dredge	SB-GC	SB-GBC	NBH dredge
Magmatic rocks	Alkali basalt and dolerite (11) Basalt, altered, undiff. (4*) *Thol. dolerite (1)* *Trachyte (1)*	Alkali basalt (3) Alkali basalt, altered (3*)	Alkali basalt (4) Alkali basalt, altered (3*)	Alkali basalt (7) *Thol. dolerite (1)* *Rhyolite (1*)*
Sedimentary rocks	Multicolored sandstone (7) Limestone (1)	Red sandstone and mudstone (2) Limestone (3)	Oolithic limestone (1)	
Metamorphic rocks	*Gneiss (2)*			*Gneiss (1)* Quartzite (4) *Hornfels (1)*

Number of samples in brackets

*Without geochemical analyses; lithologies in italics: ice-rafted debris or unclear origin

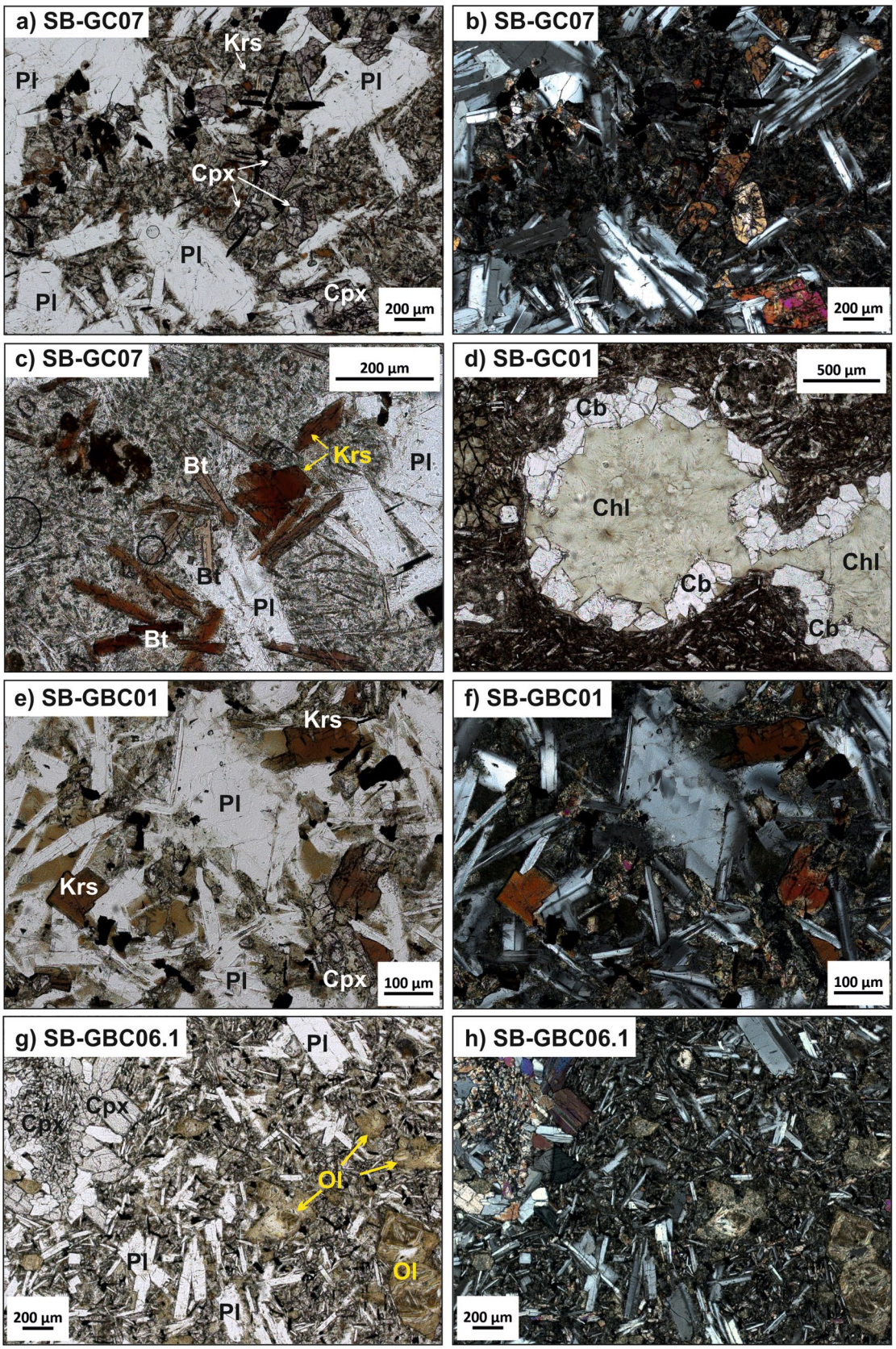
a) SB-GC07
Krs
Pl
Pl
Cpx
Pl
Pl
Cpx
200 µm
b) SB-GC07
200 µm
c) SB-GC07
200 µm
Bt
Krs
Pl
Bt
Pl
Bt
d) SB-GC01
500 µm
Cb
Chl
Chl
Cb
Cb
e) SB-GBC01
Krs
Pl
Krs
Pl
Cpx
100 µm
f) SB-GBC01
100 µm
g) SB-GBC06.1
Pl
Cpx
Cpx
Ol
Pl
Ol
200 µm
Pl
h) SB-GBC06.1
200 µm

◂ **Fig. 4** Photomicrographs of alkali basalt samples from SB-GC (**a**–**d**) and SB-GBC (**e**–**h**) as well as dated samples from the NBH dredge (**i**–**l**). **a**, **b** Hypocrystalline, seriate textured alkali basalt consisting of plagioclase, clinopyroxene (light gray-brownish), opaque minerals (Fe-Ti oxides, pyrite) and small amounts of kaersutite and biotite in a devitrified matrix. **c** Magnification of the very fine-grained matrix of the same sample to show fine-grained kaersutite and biotite crystals. **d** Amygdales filled with carbonate (rim) and greenish, spherulitic chlorite (center) in fine-grained alkali basalt. **e**, **f** Fine-grained, intersertal alkali basalt consisting of plagioclase, gray-brownish clinopyroxene, red-brown kaersutite, and opaque Fe–Ti minerals (black). PPL (**e**) and XPL (**f**). Interstices are filled with brown volcanic glass, isotropic under XPL (**f**). **g**, **h** Fine-grained, porphyritic alkali basalt composed of plagioclase, clinopyroxene (gray), and altered grains completely replaced by brownish minerals (probably former olivine) in a devitrified matrix. An ellipsoidal, ocellus-like structure (upper left corner) consists of very fine-grained clinopyroxene crystals in the center surrounded by coarser grained clinopyroxene and plagioclase. PPL (**g**) and XPL (**h**). **i**, **j** Porphyritic basalt with plagioclase phenocrysts in a fine-grained matrix of plagioclase laths, sparse clinopyroxene, and opaque and semi-opaque minerals. The latter replace mafic minerals (clinopyroxene) and volcanic glass. PPL (**i**) and XPL (**j**). **k**, **l** Very fine-grained basalt formed of plagioclase, sporadic fresh clinopyroxene and opaque and semi-opaque minerals. Phenocrysts of plagioclase and clinopyroxene (light greenish-gray) form a single glomerophyric aggregate. PPL (**k**) and XPL (**l**). *Bt* biotite, *Cb* carbonate minerals, *Chl* chlorite, *Cpx* clinopyroxene, *Krs* kaersutite, *Ol* olivine, *Pl* plagioclase. Mineral abbreviations from Whitney and Evans (2010). *PPL* plane polarized light, *XPL* crossed polarizers

et al. 1979; Brozena et al. 2003; Glebovsky et al. 2006; Gaina et al. 2009, 2017; Gernigon et al. 2012, 2020; Berglar et al. 2016; Lutz et al. 2018). At that time, Greenland was surrounded by active oceanic spreading centers in the north (Eurasia Basin), east (Norwegian–Greenland Sea), south and west (Labrador Sea–Baffin Bay) as well as by several transform faults. Due to this tectonic situation, Greenland moved northwards causing the Eurekan deformation on Ellesmere Island, along the western Svalbard margin, and in northernmost North Greenland between ca. 53 and 34 Ma (Piepjohn et al. 2016). During the Eurekan Stage 1 (anomaly 24–21, ca. 53–47 Ma), the northeastern directed drift of Greenland led to shortening along the west coast of Svalbard and the formation of the intra-continental West Spitsbergen Fold-and-Thrust Belt, as well as sinistral strike-slip along the Nares Strait (Piepjohn et al. 2016; Schneider et al. 2019). During the Eurekan Stage 2 (anomaly 21–13, ca. 47–34 Ma), Greenland moved toward the northwest causing (i) shortening across the Nares Strait and dextral strike-slip faulting on Ellesmere Island as well as (ii) dextral transpression along the major fault zones of Svalbard and the transition from oblique convergence to oblique divergence along the west Svalbard continental margin (Piepjohn et al. 2016; Kleinspehn and Teyssier 2016). At the end of Stage 2, spreading in the Labrador Sea and Baffin Bay ceased and Greenland became part of the North American plate (e.g., Srivastava and Tapscott 1986; Tessensohn and Piepjohn 2000; Piepjohn et al. 2016).

Formation and structure of the Yermak Plateau

During Eurekan Stages 1 and 2, seafloor spreading along the Gakkel Ridge terminated at the northern margin of an area that comprised the future Morris Jesup and Yermak plateaus (Engen et al. 2008). The propagation of the Gakkel Ridge toward Greenland led to the separation of the YP from the conjugate Morris Jesup Rise during the Oligocene, between ca. 33 Ma (anomaly 13) and ca. 25 Ma (anomaly 7) (Feden et al. 1979; Brozena et al. 2003; Engen et al. 2008; Ehlers and Jokat 2013).

In the Miocene, the onset of oblique rifting led to seafloor spreading along the Lena Trough propagating from north to south between ca. 21 Ma and 10 Ma (Snow et al. 2011; Jokat et al. 2016). Since about 17.5 Ma, the Fram Strait between the YP and eastern North Greenland developed into the only deep-water gateway between the Arctic Ocean and the global oceans (Jakobsson et al. 2007; Ehlers and Jokat 2013). The YP became part of the Eurasian Plate and drifted together with Svalbard apart from Greenland.

Seismic data of the YP have revealed an acoustic basement with narrow graben and horst structures, which is covered by 2 to 4 km thick Cenozoic sedimentary strata. The oldest deposits in the deeper basins may have an age of about 34 Ma (Geissler and Jokat 2004; Jokat et al. 2008; Geissler et al. 2011). The northeastern YP (Fig. 2) is characterized by positive magnetic anomalies with amplitudes up to 1000 nT following the SW–NE trend defined by the outline of the northeastern YP (Feden et al. 1979; Jackson et al. 1984; Brozena et al. 2003; Jokat et al. 2008). A seismic profile crossing the northeastern YP (line AWI-20040005; Fig. 2) revealed three basement highs, herein referred to as the northern basement highs, which are separated by grabens (Jokat et al. 2008). The northernmost and the central basement highs are associated with positive magnetic anomalies of about 750 nT and 250 nT, respectively. Only the central basement high is exposed at the seafloor. Multichannel reflection seismic data of a section along the transition from the northeasternmost margin of the YP into the oceanic Nansen Basin (line BGR13-207; Fig. 2) reveal structures typical of a rifted continental margin without any indications of subduction (Berglar et al. 2016).

The southwestern YP is magnetically quiet. A pronounced structure is the Sverdrup Bank, a flat-topped N–S trending horst structure that narrows to the north, with steep flanks to the east and west (Jokat et al. 2008; Geissler et al. 2011). Its uppermost part is composed of sedimentary and/or volcanic rocks, as indicated by *p*-wave velocities of about 4.5 km/s (Geissler et al. 2011). The Sverdrup Bank was interpreted

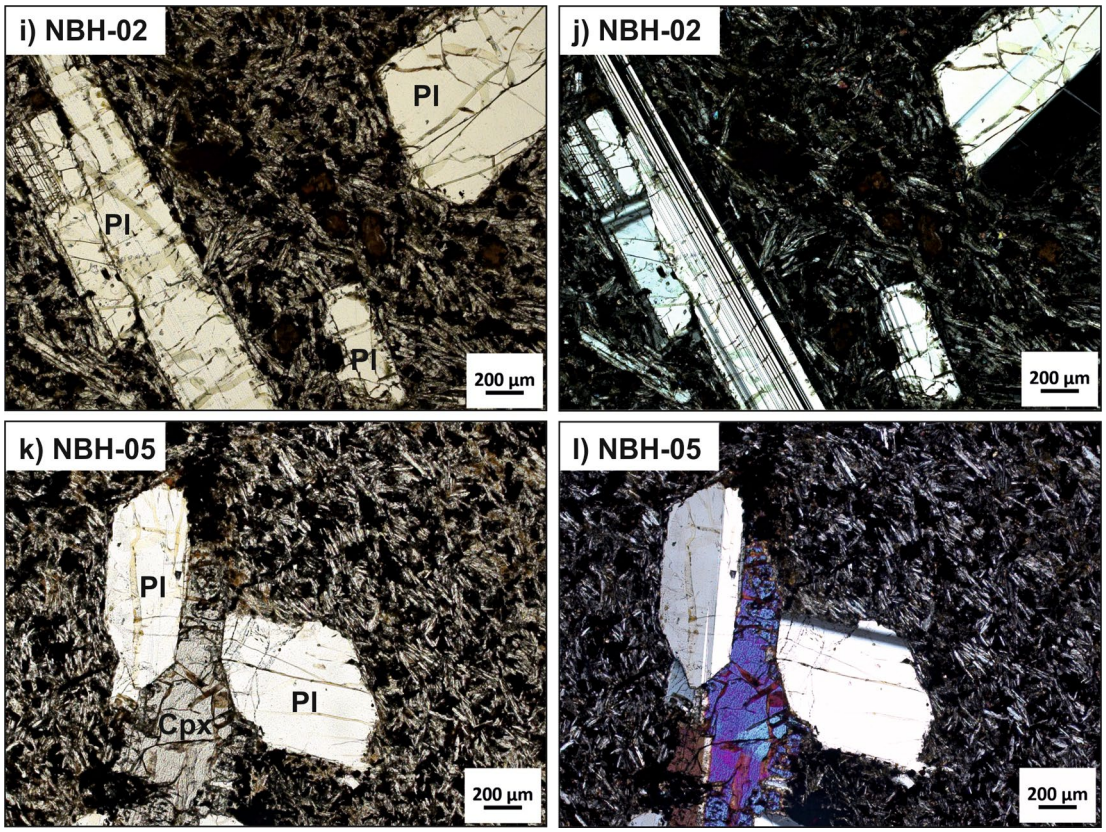

Fig. 4 (continued)

as part of a larger continental block; presumably a continuation of structures and basement rocks exposed on northern Svalbard (Ritzmann and Jokat 2003).

Samples and methods

Sampling sites and recovered materials

Sampling of basement rocks is only successful where the basement of the YP is exposed close to or at the seafloor and thus shows no (or only little) sedimentary cover. Such sites on the northern part of Sverdrup Bank (SB) and the central northern basement high (NBH) were identified by shipborne multibeam and sediment echosounder system (Stein 2005) and for each location one dredge (the SB and NBH dredges) was carried out. Beside the dredges, basement sampling on the northern part of Sverdrup Bank was also performed using (i) a gravity corer (SB-GC) on its western flank close to the SB dredge and (ii) a giant box corer (SB-GBC) on the flat top of the Sverdrup Bank around 5 km east of the SB dredge track (Fig. 2; Supplementary file 1). Cores of 32 cm and 16 cm in length were recovered from the SB-GC and SB-GBC, respectively (Supplementary file 2). From the SB-GC core, we selected eleven samples consisting of individual pebbles, of which six are basaltic and five are sedimentary. From the SB-GBC core, seven basalt samples and one sedimentary rock were collected (Table 1, Supplementary file 3). At two stations on the eastern part of the northern Sverdrup Bank (Fig. 2), no penetration with the gravity corer was possible due to the hard basement rocks at the seafloor.

Hereinafter, if the term "SB samples" is used, we refer to both, core and dredge samples from the Sverdrup Bank. If further differentiation between SB core and SB dredge is necessary, it is noted in the text.

Analytical methods

A complete list of all core and dredge samples from the YP and the applied analytical methods is given as Supplementary file 3. For this study, magmatic rock samples from the YP were analyzed using the following methods: whole-rock qualitative X-ray diffraction (XRD), whole-rock quantitative analyses of major and trace elements detected by X-ray fluorescence (XRF) and inductively coupled plasma-mass spectrometry (ICP-MS), Rb–Sr and Sm–Nd isotope analysis and $^{40}Ar/^{39}Ar$ whole-rock geochronology. For analytical details see Supplementary file 4. The XRF and ICP-MS whole-rock analytical data of the magmatic rock samples

recovered by coring (SB-GC and SB-GBC) as well as of a sample from the Alpha Ridge (PS051-041-1cc; Mühe and Jokat 2004) used for comparisons in this study can be found in the Supplementary file 5. The XRF and ICP-MS data for the SB and NBH dredge samples are given in Riefstahl et al. (2013). For graphic presentation and comparison, the major element oxides were recalculated to a loss-on-ignition (LOI) free basis. Short petrographic descriptions of samples from the NBH and SB dredges can be found in Riefstahl et al. (2013). Selected lithologies, which are important for this study, were newly examined by thin sections.

Results

Petrography

Magmatic rocks

The SB-GC and SB-GBC basaltic rock samples vary in grain size, texture, vesicularity, and degree of alteration (Fig. 4a–h). The basalts are aphyric to porphyritic, partially amygdaloidal (Fig. 4d), mostly hypocrystalline, with a fine-crystalline groundmass and partly devitrified volcanic glass in interstices (Fig. 4e, f). In some SB-GC samples, the basaltic matrix is cut by a finer-grained, few mm-thick veinlet of the same mineralogical composition as the surrounding rock. We assume that most, if not all, basaltic samples come from lava flows, which are characterized by varying textural features even in the same flow. However, it cannot be decided with certainty, whether an individual, isolated basalt pebble originated from a flow or from a small sill or dyke. Despite their textural variability, the basaltic rock samples of both cores are very similar in their mineralogical composition. Euhedral to subhedral plagioclase in the groundmass is the major mineral phase. Minor mineral phases are clinopyroxene, opaque phases, and alkali feldspar as well as dark red–brown biotite and red–brown amphibole (probably kaersutite) in some samples (Fig. 4a–c, e, f). Apatite is an accessory phase. Slightly parallel alignment of plagioclase laths in the groundmass of sample SB-GC04 is interpreted as a flow texture. Phenocrysts (up to 2 mm in size, mostly <1 mm) are slightly altered plagioclase, clinopyroxene, and pervasively altered olivine (Fig. 4g, h). Secondary phases are carbonate minerals (calcite, dolomite, traces of magnesite), chlorite, rarely pumpellyite as well as clay minerals formed from alteration of glass. The fine-grained clay minerals are muscovite or illite, which are hard to distinguish by XRD on simple powder specimens. Additionally, corrensite was detected in all samples, traces of pyrite in almost all samples and quartz, analcime and anatase in some samples (Supplementary file 6). The composition of the SB-GC and SB-GBC basalt samples shows that they have experienced hydrothermal alteration that has mainly affected olivine and interstitial volcanic glass.

The basaltic rocks are petrographically very similar to the alkali-basalt samples of the SB dredge studied by Riefstahl et al. (2013). Some coarser-grained and less altered SB dredge samples consist of plagioclase, clinopyroxene, ± alkali feldspar, ± biotite, ± dark red–brown amphibole, and ± olivine (replaced by secondary minerals). Biotite was used for Ar–Ar dating on two medium-grained samples (Riefstahl et al. 2013).

The petrographic description of the NBH alkali-basalt samples is only based on two thin sections of samples NBH-02 and NBH-05. These samples are fine-grained and strongly (NBH-02) or weakly porphyritic (NBH-05) with phenocrysts of mainly plagioclase and rare clinopyroxene. The groundmass is formed of plagioclase laths, minor clinopyroxene, abundantly dispersed opaque minerals, and rarely completely altered olivine (Fig. 4i–l). XRD measurements (Supplementary file 6) confirm a similar mineralogical composition for the other five alkali-basalt samples without thin sections, which show macroscopically a very strongly altered appearance (Riefstahl et al. 2013). In sample NBH-11, olivine was confirmed. Additionally, traces of fluorapatite were detected in in two samples. Minerals indicating alteration are only present in traces: corrensite in three samples, muscovite (or illite), and calcite in one sample each. Thus, the NBH alkali-basalt samples are only little affected by alteration, despite their altered appearance. In contrast to the SB alkali-basalt samples, the NBH basalt samples do not contain minerals as biotite and red–brown amphibole.

Non-magmatic rocks

The SB-GC and SB-GBC samples contain only a small number of sedimentary rocks represented by sandstone and limestone (Table 1). The reddish sandstone sample SB-GC03 is fine-grained, well sorted, and calcareous (Fig. 5a, b). It consists mainly of angular to subangular grains of quartz and sericitized feldspar, few green grains (mostly chlorite, also pumpellyite), detrital muscovite, rarely tourmaline, and few lithoclasts of polycrystalline quartz, sericite schist, and chlorite schist. Opaque Fe oxides and hydroxides partly form coatings of the clastic grains. Calcite commonly fills the voids. Another reddish pebble is a poorly sorted, sandy mudstone (Fig. 5c, d). Sand-sized grains are mostly angular quartz, volcanic lithoclasts, few muscovite, and rare calcite. The sample is rich in opaque, limonitic matter of probably biogenic origin. The mudstone part of the sample is rich in felted brownish fine fibers and contains some coalified plant fragments (Fig. 5e).

We consider these two samples to be associated with a prominent group of sandstone samples of the SB dredge. These medium-grained, partly silty sandstone samples are

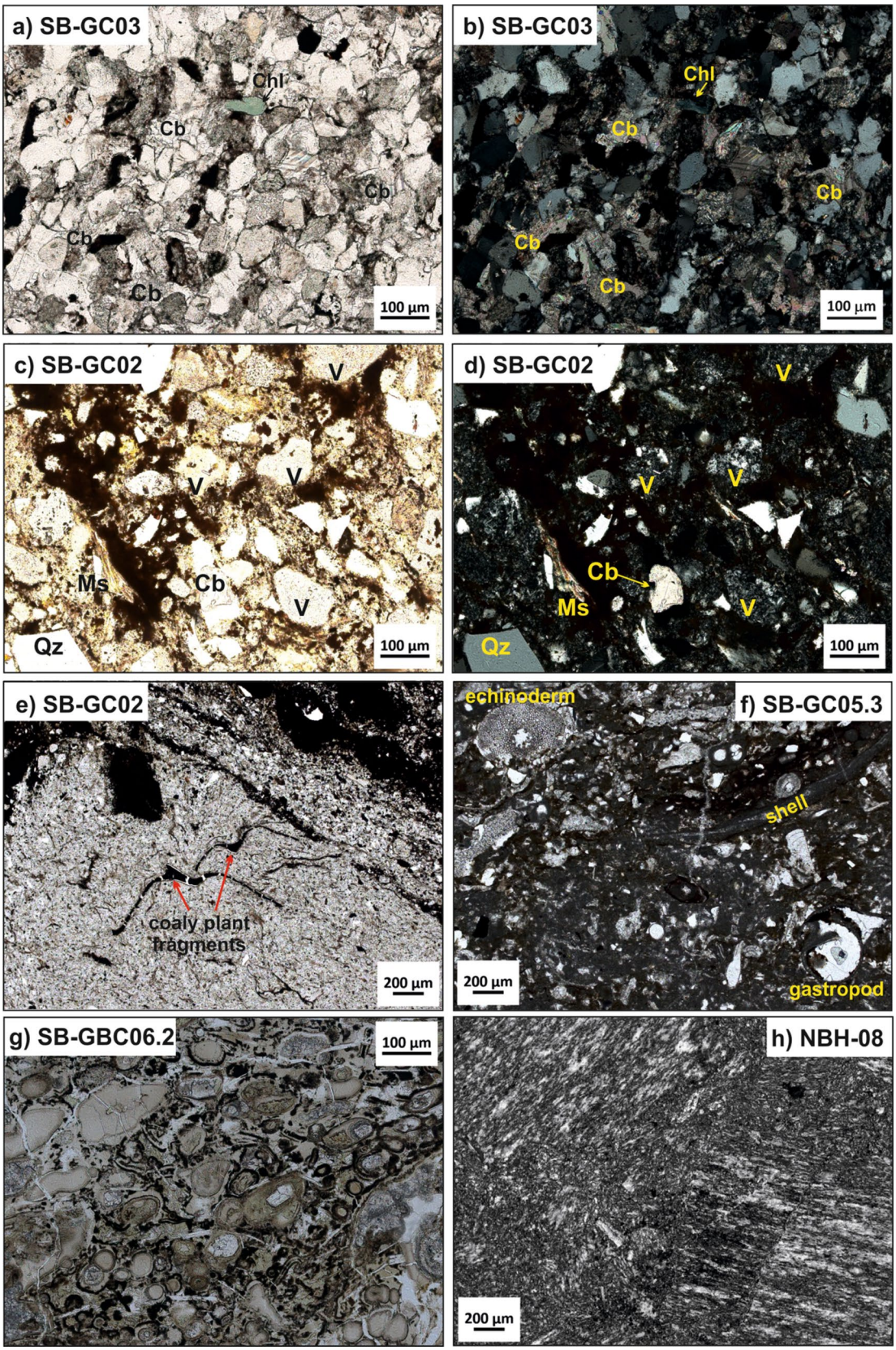
a) SB-GC03
Chl
Cb
Cb
Cb
Cb
100 µm
b) SB-GC03
Chl
Cb
Cb
Cb
Cb
100 µm
c) SB-GC02
V
V
V
Ms
Cb
V
Qz
100 µm
d) SB-GC02
V
V
V
Cb
Ms
V
Qz
100 µm
e) SB-GC02
coaly plant fragments
200 µm
f) SB-GC05.3
echinoderm
shell
200 µm
gastropod
g) SB-GBC06.2
100 µm
h) NBH-08
200 µm

◂**Fig. 5** Photomicrographs of non-magmatic rock samples from SB-GC (**a**–**f**), SB-GBC (**g**), and NBH dredge (**h**). **a**, **b** Fine-grained sandstone dominated by quartz clasts, sparse feldspar, chlorite, and lithoclasts. Opaque grains and coatings are mostly Fe oxides and hydroxides, minor grains of Ti minerals. Interspaces are filled with carbonate. PPL and XPL. **c**–**e** Layered sandy siltstone to claystone rich in limonitic opaque matter of probably biogenic origin. Sand-sized clasts are quartz and volcanic lithoclasts, minor muscovite; carbonate is sporadic (c and d; PPL and XPL). The claystone (**e**; PPL) is rich in felted fine fibers (brownish) and contains some coalified plant fragments (center, red arrows). **f** Limestone with fragments of echinoderms, gastropods, and shells in a micritic matrix (PPL). **g** Oolithic limestone (PPL). **h** Cataclastic meta-chert from the NBH dredge (XPL). The different directions of foliation of the chert fragments indicate that the ductile deformation (foliation) took place before the brittle deformation (brecciation). *Cb* carbonate minerals, *Chl* chlorite, *Ms* muscovite, *Qz* quartz, *V* volcanic lithoclast. Mineral abbreviations from Whitney and Evans (2010). *PPL* plane polarized light, *XPL* crossed polarizers

petrographically very similar to each other, despite their varying colors (dark brown, dark gray, reddish brown to red, and light gray/red–brown). The mostly angular to subangular clasts are dominantly quartz and feldspar minerals. Carbonate, mostly calcite, is always present as filling of voids, in veins, and as clastic grains. A minor, but characteristic component is represented by small green to brownish green grains, mostly formed of chlorite, sometimes pumpellyite, and glauconite. Other minor clastic components are muscovite, few lithoclasts of polycrystalline quartz, chlorite-sericite schist, volcanic rocks, as well as accessory tourmaline, zircon, and titanite. Opaque minerals, mostly iron oxides and hydroxides, form coatings of the clasts, but also appear as clastic grains. Black, round, concentric aggregates up to 1.5 mm in diameter in few samples are interpreted to be of biogenic origin.

The four SB-GC and SB-GBC limestone samples differ from each other. One of them (SB-GC05.3) is rich in fossils, such as foraminifers, gastropods, echinoderm fragments, and shale fragments, and contains abundant opaque Fe oxides and hydroxides and ca. 10% quartz in a calcareous micritic groundmass (Fig. 5f). SB-GBC06.3 is a fine to medium-grained calcareous oolithic limestone (Fig. 5g). Calcite forms the ooids and fills the voids. Furthermore, fine quartz veins, opaque minerals, and mud are present. The other limestone samples are fine-grained and rich in coarse-grained veins and lenses mainly formed of calcite and minor quartz. They also contain few opaque minerals and traces of chlorite.

The NBH dredge does not contain sedimentary rocks, but a group of quartzite samples (Table 1). The quartzites comprise two dark-banded, foliated samples (NBH-03, -09) and two light gray, cataclastic samples (NBH-07, -08). The foliation is defined by fine-grained elongated quartz aggregates and thin aligned muscovite flakes. Sample NBH-03 is a strongly foliated rock with rare porphyroclasts and a simple shear flow pattern indicating a mylonitic deformation (see Fig. 5A in Riefstahl et al. 2013). The cataclastic quartzites contain angular fragments with an internal foliation, showing that the ductile deformation took place before the brittle deformation (Fig. 5h). Despite their different appearance and textures, the mineralogical and geochemical composition of the mylonitic and cataclastic quartzites is very similar. They are mainly formed of recrystallized quartz with only small amounts of muscovite, few opaque and zircon grains. Their major element composition is dominated by 96–99 wt% SiO_2, with up to 2.2 wt% Al_2O_3, 1.6 wt% Fe_2O_3, 0.6 wt% K_2O, while the other major element oxides are < 0.2 wt% (Riefstahl et al. 2013). Such pure quartzites originate most likely from chert formed by biogenic or chemical processes with only a small amount of clastic input (for comparison see analytical data, e.g., from Cressman 1962 and Wang et al. 2012). In the following, these samples are referred to as meta-chert.

$^{40}Ar/^{39}Ar$ geochronology of alkali-basalt samples from the NBH dredge

Basalt samples NBH-02 and NBH-05 were selected for Ar–Ar whole-rock geochronology (Fig. 6, Supplementary file 8). Sample NBH-02 yielded an age spectrum with a four-step plateau (in total 9 temperature steps), which is characterized by 51.0% of the released ^{39}Ar and an age value of 92.5 ± 1.8 Ma (2σ). Sample NBH-05 also yields an age spectrum with a four-step plateau (in total 8 temperature steps) characterized by 59.6% of the released ^{39}Ar and an age value of 104.5 ± 2.2 Ma (2σ). The Ca/K ratios of both samples are relatively constant through the spectrum, and increase only in the highest temperature step in each sample (NBH-02: 3.92–19.61; NBH-05: 3.4–9.31). Both samples show linear trends on the inverse isochron plots (Fig. 6) with age values of 98.2 ± 5.8 Ma (2σ) for NBH-02 and 102.4 ± 5.8 Ma (2σ) for NBH-05. The initial $^{40}Ar/^{36}Ar$ ratios of both samples overlap or are close to the modern atmospheric ratio of 295.5 within 2σ uncertainty. The plateau age, the inverse isochron age, and the total fusion age of each sample overlap within 2σ uncertainty and can be considered geologically meaningful.

Since the inverse isochron ages of both samples have lower MSWDs, are closer together, and overlap within 2σ uncertainty, we prefer these ages (with an average of around 100 Ma) for further interpretation. The overlapping age interval of ca. 104 to 97 Ma is interpreted to be the best estimate for the NBH alkaline basalts.

Obtaining whole-rock Ar–Ar ages from basaltic samples with indications of alteration is difficult. However, the obtained ages correspond to the middle Cretaceous (late Albian to Turonian) and are clearly different from the ca. 51 Ma age of the alkaline basalts from the SB dredge

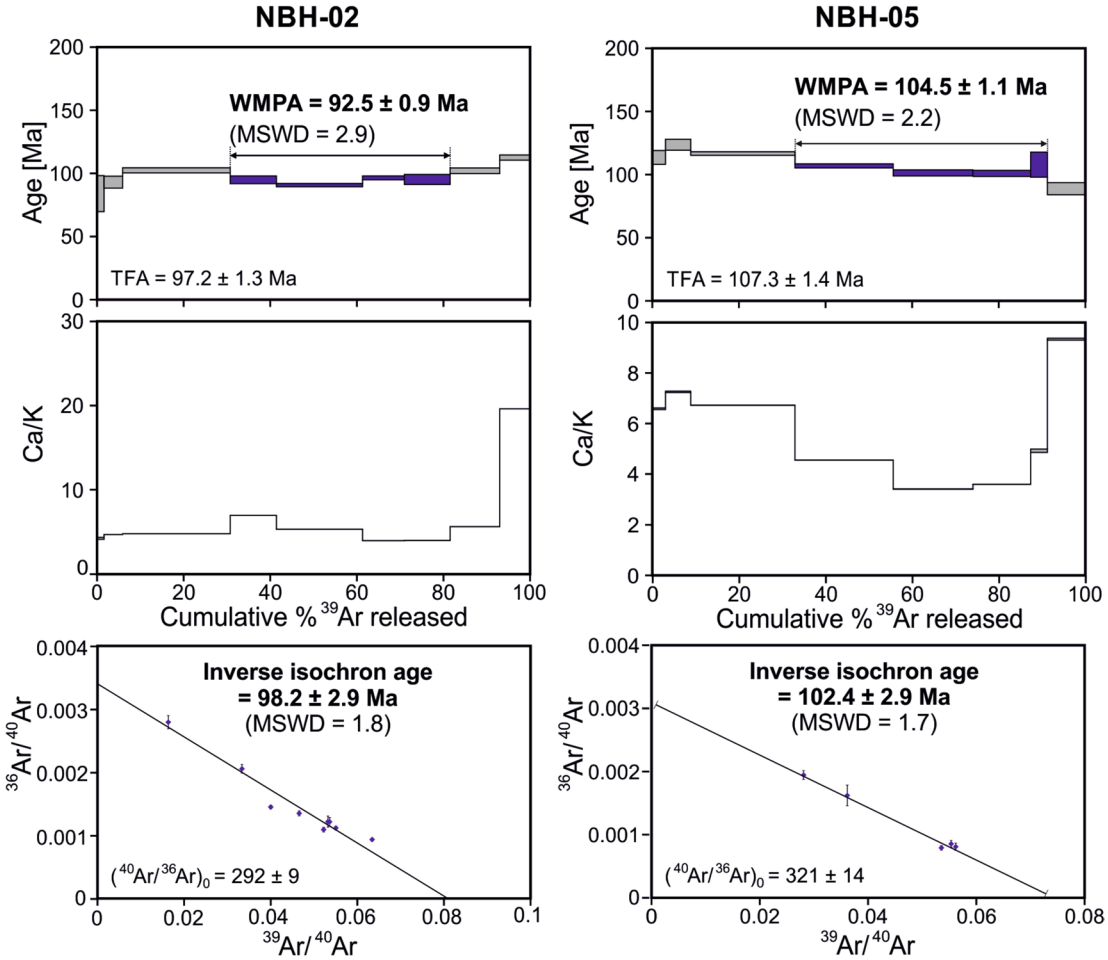

Fig. 6 $^{40}Ar/^{39}Ar$ age plots for whole-rock basalt samples NBH-02 (left) and NBH-05 (right). Errors in ages and initial Ar isotope ratios are reported as 1σ values (including error in J value). *MSWD* mean standard weighted deviation, *TFA* total fusion age, *WMPA* weighted mean plateau age

(Riefstahl et al. 2013). They also differ from the Early Cretaceous Ar–Ar ages (144–133 Ma) of the tholeiitic dolerite samples from the SB and NBH dredges (Riefstahl et al. 2013). The age interval of 104 to 97 Ma indicates that the area of the northeastern YP was affected by basaltic volcanism during the second main pulse of HALIP volcanism.

Whole-rock geochemistry of the basaltic samples

Alkaline basalt samples

In all sample localities, alkaline basaltic rocks are present (Table 1). The core samples have relatively high LOI values (4.0–11.6 wt%; Supplementary file 5). The LOI-free calculated major element concentrations of the SB-GC and SB-GBC samples vary in a relatively narrow range: 47.1–52.3 wt% SiO_2, 1.8–2.3 wt% TiO_2, 16.9–20.1 wt% Al_2O_3, 6.2–9.0 wt% total Fe_2O_3, 3.6–8.8 wt% MgO, 7.5–15.0 wt% CaO, 2.1–3.2 wt% Na_2O, 1.9–4.0 wt% K_2O, and 0.49–0.88 wt% P_2O_5. Sample SB-GC07 shows the highest SiO_2, Al_2O_3, K_2O, as well as lowest MgO and total Fe_2O_3 concentrations of the suite, probably an effect of magma differentiation (Supplementary file 7).

With this major-element composition, the SB-GC and SB-GBC samples are in the range of the alkali-basalt samples from the SB dredge: 39.8–51.4 wt% SiO_2, 1.7–2.2 wt% TiO_2, 15.6–20.2 wt% Al_2O_3, 5.8–9.7 wt% total Fe_2O_3, 3.6–9.2 wt% MgO, 6.6–21.1 wt% CaO, 2.2–5.0 wt% Na_2O, 1.6–4.2 wt% K_2O, and 0.40–0.85 wt% P_2O_5 (Supplementary file 7). Some of the SB dredge samples have higher CaO and LOI contents than the core samples due to carbonate filling of vesicles and spilitization.

The NBH alkali-basalt samples differ from the SB samples mainly by higher TiO_2 and total Fe_2O_3 concentrations

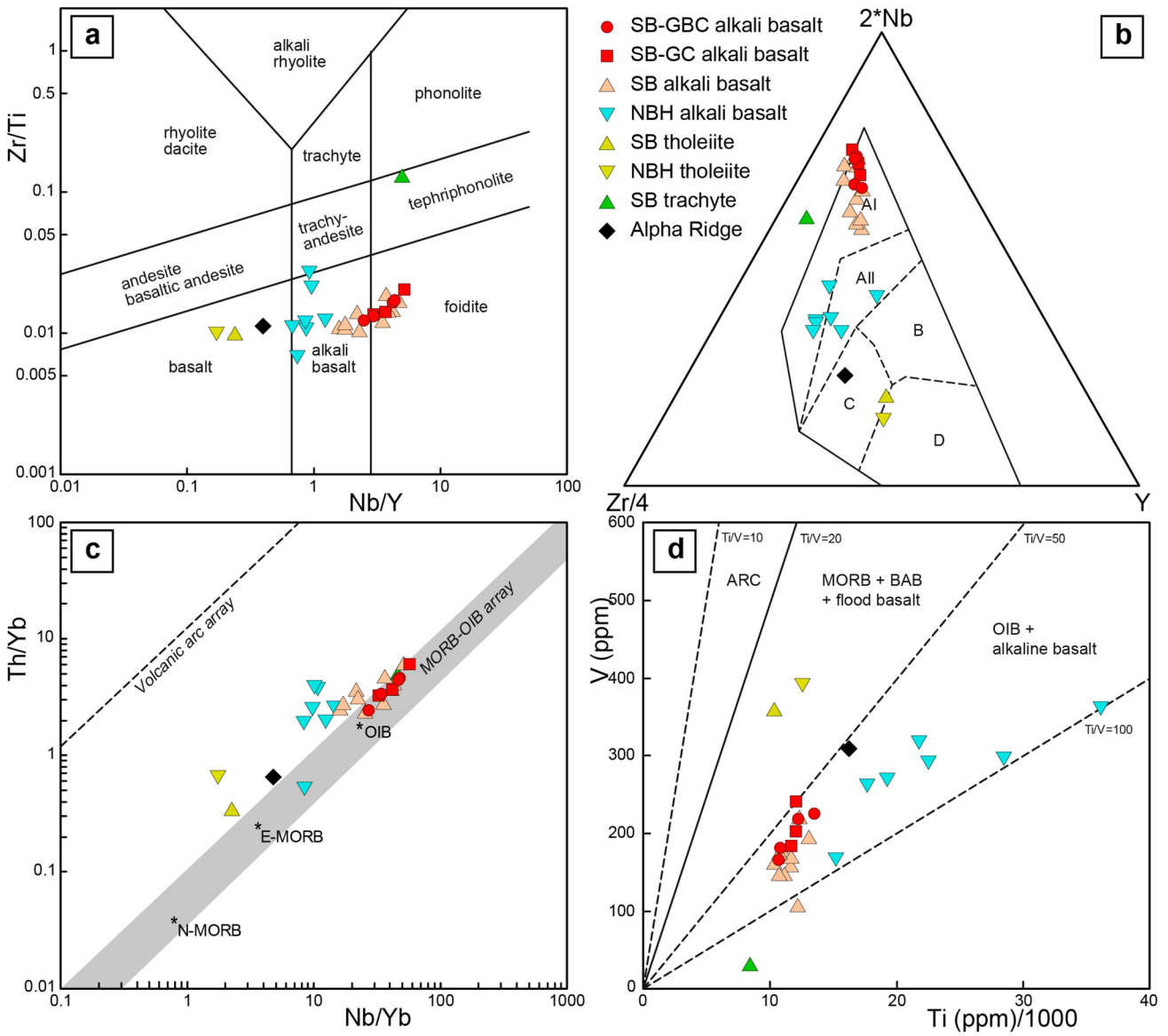

Fig. 7 Geochemical variation diagrams for magmatic rock samples from SB-GC core, SB-GBC core, SB dredge, and NBH dredge of the YP as well as a basalt sample from the Alpha Ridge. Data sources: SB-GC and SB-GBC—this study (Supplementary file 5), SB and NBH dredge samples (triangle-shaped symbols—Riefstahl et al. 2013), Alpha Ridge sample—unpublished data from Mühe and Jokat (2004) (see Supplementary file 5). **a** Zr/Ti versus Nb/Y classification diagram from Pearce (1996). **b** 2*Nb-Y-Zr/4 geotectonic discrimination diagram (Meschede 1986). Fields: within-plate alkali basalt—AI, AII; within-plate tholeiite basalt—AII, C; P-type MORB—B; N-type MORB—D; Volcanic arc basalt—C, D. **c** Th/Yb versus Nb/Yb diagram from Pearce (2008). Values for N-MORB, E-MORB, OIB are from Sun and McDonough (1989). Crustal input is indicated for samples plotting above the MORB–OIB array. **d** V versus Ti diagram from Shervais (1982). *ARC* Island arc tholeiite basalts, *MORB* Mid-ocean ridge basalts, *N-MORB* normal MORB, *E-MORB* enriched MORB, *BAB* Back-arc basalts, *OIB* Ocean island basalts

(Supplementary file 7). Sample NBH-13 plots into the trachyandesite field of the TAS diagram (Supplementary file 7). The sample with the highest MgO (5.1 wt%), NBH-02, also has the highest Fe_2O_3 (17.3 wt%) and P_2O_5 (1.73 wt%) concentrations.

To minimize the influence of alteration effects, the magmatic samples are characterized using trace elements, which are relatively immobile during such processes. The SB-GC and SB-GBC samples can be characterized as alkaline within-plate basalts using the diagrams from Pearce (1996) and Meschede (1986) (Fig. 7a, b). The high Nb/Y ratios of the SB-GC and SB-GBC samples (2.48–5.18) and SB dredge samples (1.58–4.78) are typical for alkaline basalts (Nb/Y > 0.67; Winchester and Floyd 1977). The NBH samples with lower Nb/Y ratios of 0.68–1.23 can be characterized as mildly alkaline basalts (Fig. 7a).

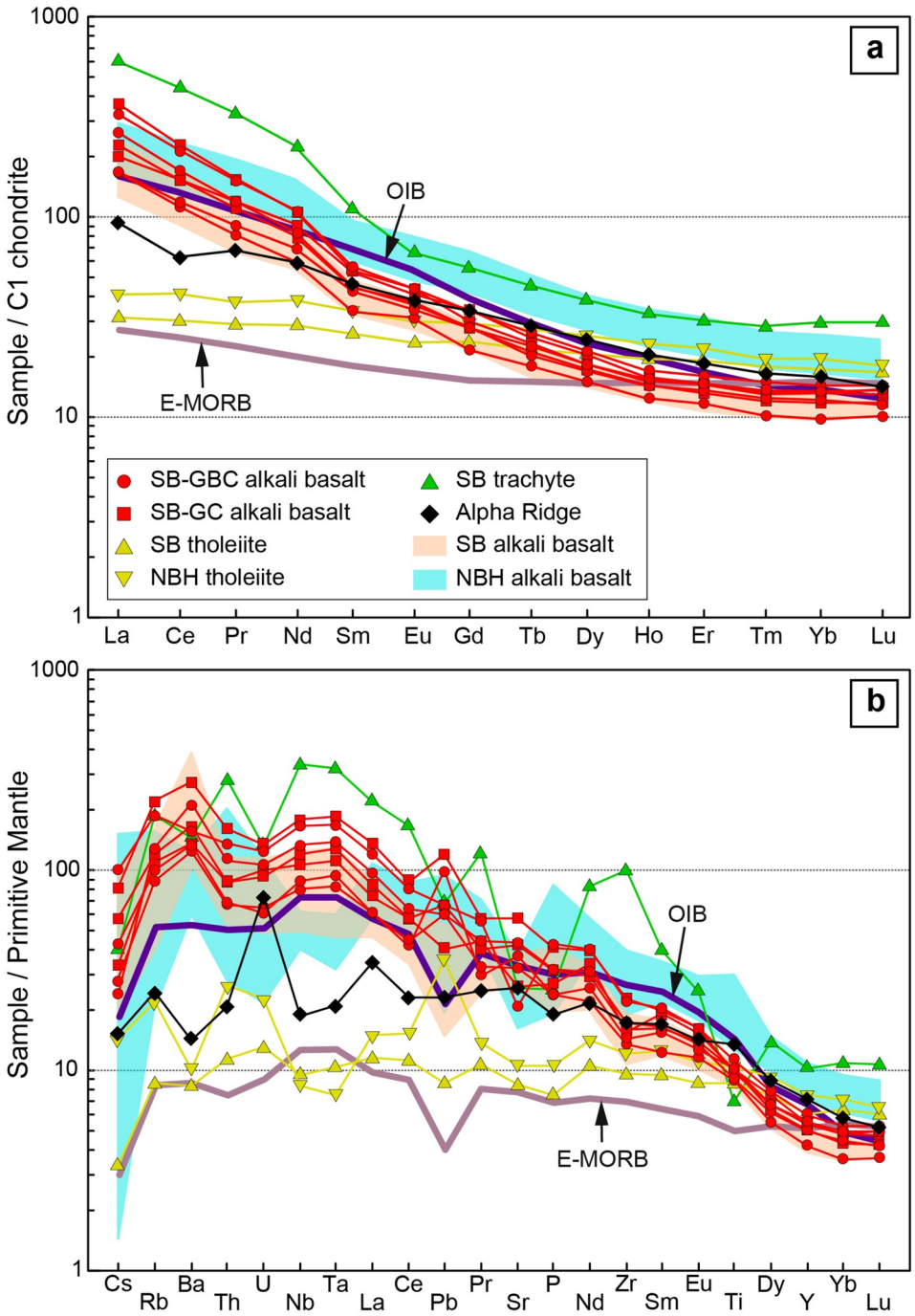

Fig. 8 **a** Chondrite-normalized rare-earth element (REE) plot and **b** primitive-mantle (PM) normalized incompatible trace element plot for magmatic samples from the YP and a basalt sample from the Alpha Ridge. Data sources as Fig. 7. C1-chondrite, OIB, and E-MORB from Sun and McDonough (1989), PM from McDonough and Sun (1995)

Geochemical affinity of the SB-GC and SB-GBC samples to oceanic-island basalts (OIB) and alkaline basalts, including continental rift-related, is shown in the Nb/Yb vs. Th/Yb diagram from Pearce (2008) and the Ti–V diagram from Shervais (1982) (Fig. 7c, d). In all diagrams, the SB-GC, SB-GBC, and the SB dredge samples overlap. The mildly alkaline NBH samples also show within-plate and OIB characteristics; however, their data points are clearly separated from the SB samples and follow different trends (Fig. 7). Most NBH samples (apart from NBH-02) plot above the MORB–OIB array at higher Th/Yb ratios indicating contamination by continental crust (Fig. 7c).

On a chondrite-normalized rare-earth element (REE) diagram, the SB-GC and SB-GBC samples show mostly parallel, OIB-like patterns with a negative slope ($La_n/Lu_n = 12.7–27.8$) and flattening in the range of the heavy REE ($Dy_n/Yb_n = 1.39–1.58$) relatively to the OIB pattern ($Dy_n/Yb_n = 1.74$). They overlap the field of SB dredge alkali basalts ($La_n/Lu_n = 11.2–23.6$; $Dy_n/Yb_n = 1.36–1.53$) (Fig. 8a). Only samples SB-GBC02.1 and SB-GBC02.2

are more enriched in the light REEs (La–Pr). In contrast, the field of the NBH alkali basalts has a flatter negative slope ($La_n/Lu_n = 6.6–13.2$) but steeper heavy REEs ($Dy_n/Yb_n = 1.60–2.28$). The chondrite-normalized REE values of the NBH basalts are generally higher than OIB and are also higher than the Sm to Lu values of the SB samples.

On a primitive-mantle-normalized trace element diagram, the SB-GC and SB-GBC samples show mostly parallel patterns, which overlap with the field of the SB dredge alkaline basalts and follow the OIB trend (Fig. 8b). The SB samples show a pronounced positive Nb–Ta anomaly (relative to La and U) typical for OIB, and a small negative Zr peak. In contrast, the NBH alkali basalts, which also show OIB-like patterns and partly overlap with the SB samples, are more enriched in the range of Zr to Lu and have a negative Nb–Ta anomaly (relative to La and U). Consequently, the Zr/Nb ratios of the SB samples (Zr/Nb = 2.01–3.64) and of the NBH samples (Zr/Nb = 5.76–10.83) are very different.

Tholeiitic basalt samples

Our dataset comprises three tholeiitic basalt samples: one dolerite sample each from the SB dredge (SB-07) and the NBH dredge (NBH-01), (Riefstahl et al. 2013), as well as the basalt sample from the Alpha Ridge (Jokat et al. 2013). All these samples have low Nb/Y ratios (Fig. 7a), plot within or close to the fields of within-plate tholeiites and continental flood basalts (Fig. 7b, d), and show affinity to E-MORB with indications of crustal contamination (Fig. 7c). The tendency toward E-MORB is supported by the chondrite-normalized REE patterns of the two YP dolerite samples with a very flat negative slope ($La_n/Lu_n = 1.93–2.15$), whereas the pattern of the Alpha Ridge sample is steeper ($La_n/Lu_n = 6.8$) and its strongly fractionated heavy REE ($Dy_n/Yb_n = 1.58$) show a tendency to OIB (Fig. 8a). The primitive-mantle normalized patterns of the tholeiitic samples are relatively flat, however with distinct negative Nb–Ta anomalies indicating involvement of a continental crustal component (Fig. 8b). The pronounced positive U peak of the Alpha Ridge sample together with the negative Ce anomaly (Fig. 8a) can be a result of low-temperature seafloor alteration (e.g., Staudigel et al. 1996; Beier et al. 2011). A similar behavior of Ce and U is reported from a basalt sample dredged from the Mosby Seamount in the Sophia Basin (Fig. 2; Geissler et al. 2019). The strong alteration has also affected the major-element composition of the Alpha Ridge sample showing very low concentrations of MgO (0.96 wt%) and Fe_2O_3 (5.21 wt%), but a very high Al_2O_3 content (26.04 wt%) indicating decomposition of mafic minerals and their replacement by clay minerals.

Sr and Nd isotope data

The samples analyzed for Sr and Nd isotope data represent the major types of magmatic rocks from the dredges: the alkaline basalt group of the SB dredge with an age of 51 Ma, the mildly alkaline basalts from the NBH dredge with an age of ca. 100 Ma, and the two tholeiitic dolerite samples (one from each dredge) with Early Cretaceous ages of 144 and 133 Ma. These ages are used to calculate the initial Sr and Nd isotope ratios (Fig. 9, Supplementary file 9).

The differences in the geochemical signatures and the age between the alkaline basalts from the SB dredge and the mildly alkaline basalts from the NBH dredge are also manifested in the different Nd isotope ratios and potentially also in the Sr isotope data (only one analysis for each group available). The alkaline basalts from the SB dredge have relatively high initial $\varepsilon Nd(t)$ values in the range of +4.9 to +3.1 and a low initial $(^{87}Sr/^{86}Sr)_t$ ratio of 0.7037 (from sample SB-04 with $\varepsilon Nd(51\ Ma) = 4.5$). The mildly alkaline NBH basalts show mostly lower initial $\varepsilon Nd(t)$ values in the range of +3.7 to +0.1 and a higher initial $(^{87}Sr/^{86}Sr)_t$ ratio of 0.7054 (from sample NBH-02 with $\varepsilon Nd(100\ Ma) = 2.3$). Both tholeiitic dolerite samples (SB-07, NBH-01) have relatively primitive initial $\varepsilon Nd(t)$ values (4.1 and 5.5) and initial $(^{87}Sr/^{86}Sr)_t$ ratios of 0.7046 and 0.7049.

The Nd model ages (t_{DM}) of the three basalt groups are also different. The alkaline basalts from the SB dredge have the lowest model ages of 0.32 to 0.49 Ga, whereas the t_{DM} values of the mildly alkaline NBH basalts range between 0.59 and 0.85 Ga and overlap in parts with the values of the two tholeiitic dolerites of 0.76 and 1.02 Ga. These higher t_{DM} ages indicate contamination with old continental crust.

Discussion

In-situ rocks versus ice-rafted debris

During the late Quaternary glaciations, large parts of North America, northern Europe, and Asia were covered by ice (e.g., Jakobsson et al. 2010, and references therein). The Eurasian ice sheet reached the northern margin of the Barents Shelf and also covered the YP during the Saalian glaciation (e.g., Svendsen et al. 2004; Spielhagen et al. 2004). Glaciogenic features, such as mega-scale lineations and iceberg plow marks, were identified on almost the entire YP (e.g., Vogt et al. 1994; Dowdeswell et al. 2010; Gebhardt et al. 2011; Jakobsson et al. 2014). The Transpolar Drift, the major oceanic current in the Eurasia Basin, transports surface water, sea ice, and icebergs including ice-rafted debris of clay to boulder size from the East Siberian Sea, Laptev Sea, and Kara Sea and passes the YP on its way toward

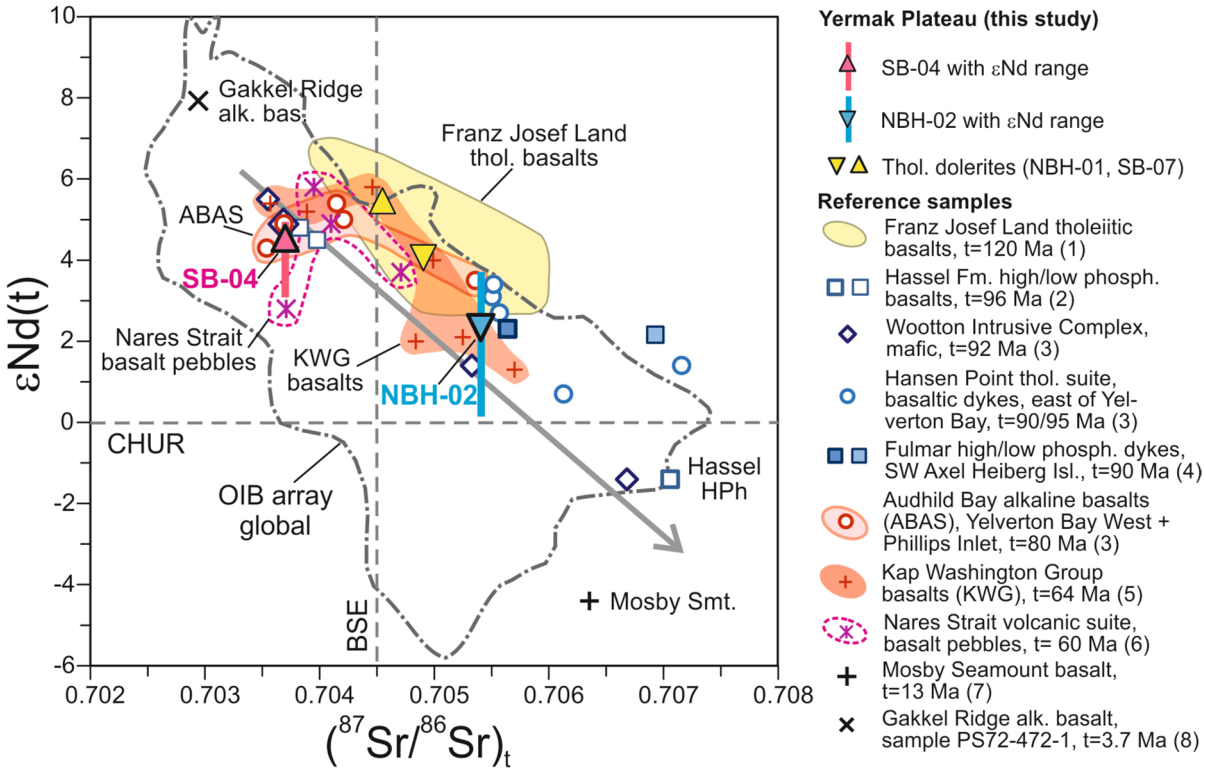

Fig. 9 Sr–Nd isotope variation diagram for basalt samples dredged from the YP. The blue and red vertical bars show the range of the εNd(*t*) values without $(^{87}Sr/^{86}Sr)_t$ data. Reference data of geochemically and/or chronologically similar basaltic rocks from surrounding areas are shown for comparison (see Figs. 1 and 3 for location): basalts from Franz Josef Land, Ellesmere Island (Hassel Formation high and low phosphorus basalts, Wootton Intrusive Complex, Hansen Point tholeiitic suite, Audhild Bay alkaline suite, Nares Strait volcanic suite), Axel Heiberg Island (Fulmar high and low phosphorus dykes), and North Greenland (Kap Washington Group). Yellow symbols and field indicate age of magmatism > 120 Ma, blue symbols are for ages of ca. 100–90 Ma, and reddish symbols and fields are for ca. 80–50 Ma. Samples from the Mosby Seamount (Sophia Basin) and from the easternmost Gakkel Ridge are also shown (black symbols). Data sources are given in brackets: (1) Ntaflos and Richter (2003); (2) Estrada (2015); (3) Estrada et al. (2016); (4) Bédard et al. (2021a); (5) Estrada et al. (2001); (6) Estrada et al. (2010); (7) Geissler et al. (2019); (8) Jokat et al. (2019). The global OIB array is from Hofmann (2003). The thick gray arrow (trend 1 from Estrada et al. 2016) represents a mixing trend between an OIB-like mantle source and granulite-facies lower crust or a lithospheric mantle component. *BSE* Bulk Silicate Earth, *CHUR* Chondritic uniform reservoir, *OIB* Ocean island basalt

the Fram Strait (Phillips and Grantz 2001; Spielhagen et al. 2004). Middle Pliocene sediments of the YP are sourced from the Laptev Sea and Kara Sea with some input from the Barents Sea as detected by heavy mineral studies (Strand et al. 2008).

Thus, the presence of ice-rafted clasts in dredges and cores from the YP cannot be excluded, even if these rocks were recovered on basement highs without significant sedimentary cover. Riefstahl et al. (2013) tried to distinguish between ice-transported rocks and in situ basement rocks in the samples dredged from the YP. A trachyte sample from the SB dredge dated at 249 Ma by apatite (U-Th-Sm)/He thermochronology was identified to be ice-rafted from the Siberian trap province. The two tholeiitic dolerites with Early Cretaceous Ar–Ar ages, one each from the SB and NBH dredge, were interpreted to originate from Franz Josef Land (Riefstahl et al. 2013). However, most of the dredge samples were interpreted as in situ rocks from the basement of the YP (Table 1). This is supported by the results of this study. The alkali-basalt samples from the SB-GC and SB-GBC cores and the SB dredge of the Sverdrup Bank are very similar in their mineralogical composition and geochemical signatures permitting all samples to be related to the same volcanic suite. The Ar–Ar biotite age of 51 Ma, obtained on SB dredge samples (Riefstahl et al. 2013), is hence presumably representative for the whole suite. The alkali-basalt samples from the NBH dredge with a mid-Cretaceous Ar–Ar whole-rock age of ca. 100 Ma (Fig. 6) differ clearly from the alkali-basalt suite of the Sverdrup Bank also in the mineralogy, geochemistry, and Sr–Nd isotopy (Figs. 7, 8, 9).

The alkali basaltic samples of both localities are associated with specific non-magmatic lithologies. The dredge and core samples of the Sverdrup Bank comprise red and gray sandstones, which are petrographically very similar, as well

as several limestone samples. Such lithologies are not present in the NBH dredge (Table 1). Instead, the NBH dredge contains a small group of meta-chert samples. All these alkali-basalt and non-magmatic samples are most probably in situ rocks from the basement of the YP. The systematic accumulation of rock fragments of specific lithologies by ice transport is highly unlikely. However, the ice-transported or in situ origin of a few gneiss samples recovered by both dredges, as well as the origin of a hornfels sample and a very small rhyolite sample from the NBH dredge (Table 1) stays unclear without additional analyses.

Plate-tectonic constraints for the northeastern Yermak Plateau: a crustal fragment from North America?

The mildly alkaline NBH basalts with an estimated age of ca. 100 Ma are part of the magmatic rocks, which presumably cause the positive magnetic anomalies of the northeastern YP (Fig. 2a). At the time of magmatism, the area of the future Yermak and Morris Jesup plateaus was a part of the passive continental margin of the developing Amerasia Basin with a position close to North Greenland, the northeastern Canadian Arctic, and Svalbard with a paleogeographic position northeast of Greenland. These areas were affected by Cretaceous HALIP-related magmatism. In Svalbard and Franz Josef Land, Early Cretaceous tholeiitic mafic magmatism related to the first pulse of the HALIP is dominant. U–Pb dating of a few sill and tuff samples yielded ages of ca. 125 to 122 Ma (Corfu et al. 2013). Despite the frequent occurrence of Early Cretaceous igneous intrusions on Svalbard, no clear description of a mid-Cretaceous alkaline magmatic occurrence is available in the literature (cf. Senger et al. 2014; Senger and Galland 2022).

In the Lake Hazen area of northeast Ellesmere Island, Canadian Arctic, and North Greenland (Fig. 3), alkaline basaltic suites show common characteristic geochemical features. They comprise low-phosphorus and high-phosphorus members, with the latter additionally showing positive anomalies of Ba and Eu, and a negative anomaly of Zr in primitive-mantle normalized plots (Fig. 10). This concerns basalts within the Cenomanian Hassel Formation with Ar–Ar ages of ca. 96 Ma (Osadetz and Moore 1988; Estrada 2015), and the northeastern part of a swarm of alkaline dykes and sills of the recently defined Fulmar Suite (Bédard et al. 2021a) in the Lake Hazen area, as well as the younger Peary Land alkaline basaltic dykes in North Greenland with U–Pb ages of ca. 81–82 Ma (Thórarinsson et al. 2015) and Ar–Ar ages around 85 Ma (Kontak et al. 2001). The typical P–Ba–Eu enrichment is also present in basalts of the alkaline bimodal Kap Washington Group with U–Pb ages in the range of 71–61 Ma at the northernmost margin of North Greenland (figures in Thórarinsson et al. 2011).

Such geochemical features are present in the mildly alkaline NBH basalt samples (Fig. 10). Sample NBH-02 is a high-phosphorus basalt (1.73 wt% P_2O_5) with moderate Ba concentration (573 ppm) and a small positive Eu anomaly (Eu/Eu* = 1.17). Sample NBH-05 (together with the other NBH samples of this group) does not show the P–Ba–Eu enrichments und coincides well with the low-phosphorus members of the other basalt suites. The only differences are the higher Th, U, and Pb values of NBH-05, which can be explained by continental crustal contamination, which is also indicated from the Nb/Yb–Th/Yb diagram (Fig. 7c). Veins with apatite, carbonate minerals and Ba-Ti-oxides within the metasomatized subcontinental lithospheric mantle beneath the continental crust of North Greenland and northeastern Ellesmere Island are discussed as a possible source for the characteristic P–Ba–Eu enrichments (Bédard et al. 2021a). These basaltic suites were probably generated from a similar heterogeneous, metasomatically enriched lithospheric source. This could imply a possible common deeper crustal relationship of the areas of the northeastern YP, North Greenland, and northeastern Ellesmere Island at the time of magmatism.

Similarities in the crustal structure beneath northeast Ellesmere Island and the North Greenland shelf are also indicated by deep seismological data: a N–S trending crustal transect crossing Ellesmere Island constructed from receiver function data (Schiffer et al. 2016; Schiffer and Stephenson 2017) and a ca. 100-km-long seismic refraction line (BGR18-1R1) running from north of Kap Washington toward the southwestern edge of the Morris Jesup Spur (Brotzer et al. 2022) (Fig. 3). On northeast Ellesmere Island, the crustal structure beneath the Lake Hazen area is characterized by a ca. 15 km thick layer of metasedimentary rocks of the deep-water sequence of the Paleozoic Franklinian Basin. The seismic velocity model for the North Greenland shelf shows an offshore continuation of the deformed deposits of the Franklinian Basin up to the margin of Morris Jesup Spur. A high-velocity lower crustal layer at the boundary to the Moho was recorded in both profiles and interpreted as magmatic underplating or intrusion of sills (Schiffer and Stephenson 2017; Stephenson et al. 2017; Brotzer et al. 2022). This lower crustal layer might have contributed to the metasomatism of the lower crust (the Archean to Proterozoic Greenland–Canadian Shield) and the subcontinental lithospheric mantle, and thus led to the unusual elemental enrichments of the Cretaceous alkaline basaltic melts.

The similarity in the crustal structure beneath northeast Ellesmere Island and the North Greenland shelf allows proximity of these crustal regions during the time of Cretaceous magmatism. Since the northeastern YP represents the conjugate margin of the Morris Jesup Spur, it can be speculated that this also applies to the YP. Therefore, we suggest that northeast Ellesmere Island, North Greenland, and probably

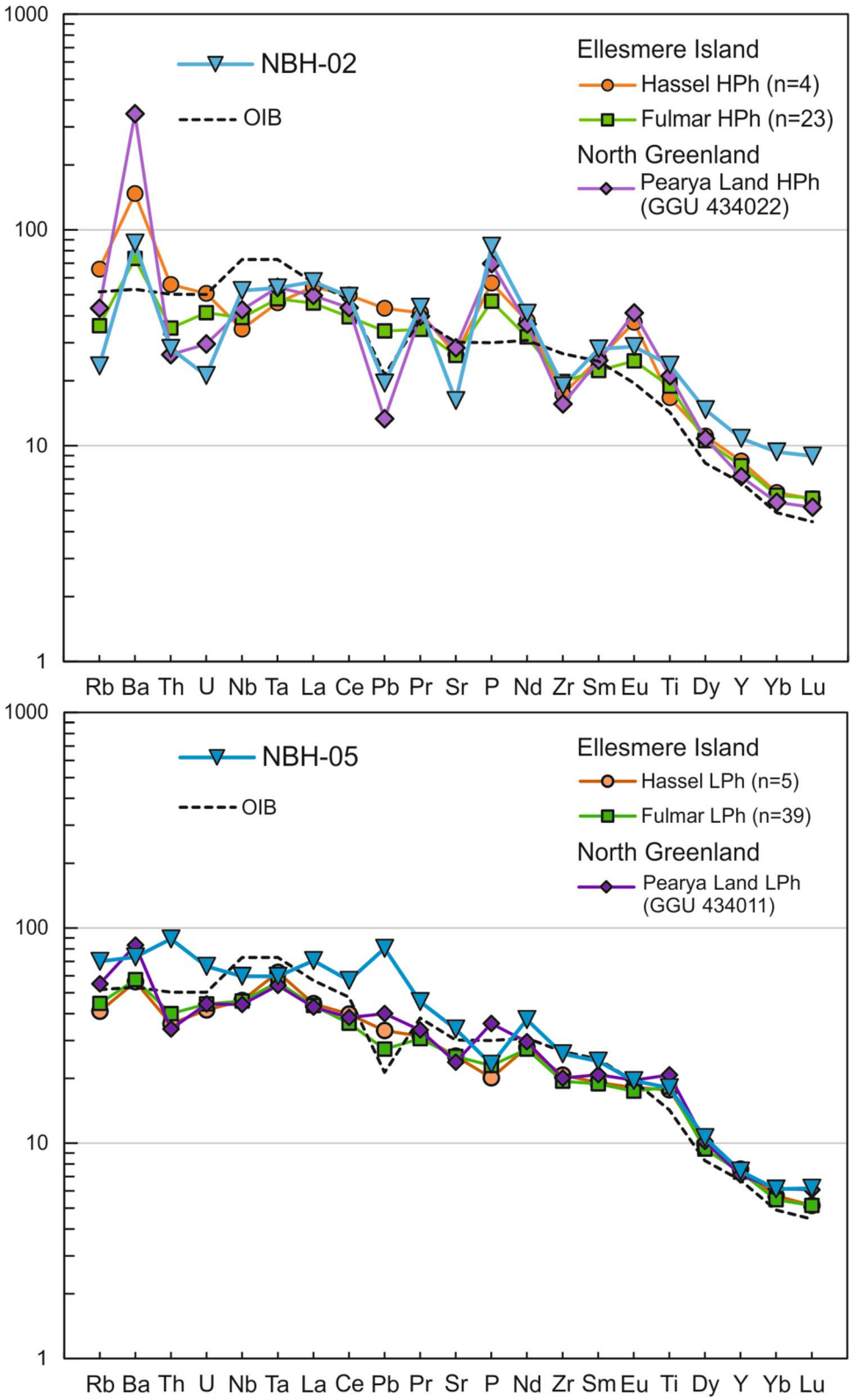

Fig. 10 Comparisons of primitive-mantle (PM) normalized incompatible trace element concentrations of a high-phosphorus (NBH-02) and a low-phosphorus (NBH-05) basalt sample from YP with similar basaltic rocks from Ellesmere/Axel Heiberg islands and North Greenland. High-phosphorus (HPh) basaltic rocks are characterized by positive P, Ba and Eu anomalies (above) in contrast to the associated low-phosphorus (LPh) basalts (below). Data of the NBH samples are from Riefstahl et al. (2013), of the Hassel Formation basalts exposed in the Lake Hazen area of northern Ellesmere Island are from Estrada (2015), of the Fulmar basalt dykes and sills in south to southeast Axel Heiberg Island and western to north-eastern Ellesmere Island from Bédard et al. (2021a), and of the Peary Land dykes in North Greenland from Kontak et al. (2001). PM from McDonough and Sun (1995), OIB from Sun and McDonough (1989)

the northeastern YP and the Morris Jesup Rise were underlain by continental crust of similar composition at the time of Cretaceous magmatism.

The presumed connection of the basement of the northeastern YP with northeast Ellesmere Island and North Greenland prior to its separation from the Morris Jesup Rise requires a new consideration of the metamorphic rock clasts in the NBH dredge (Table 1). Four samples of quartzite, now identified as meta-chert, and a single gneiss sample were previously interpreted as in situ rocks of the northeastern YP basement, which was considered as a continuation of pre-Devonian units exposed on northern Svalbard (Riefstahl et al. 2013). The presence of meta-chert pebbles does not necessarily require a connection to Svalbard. In North Greenland, chert is present in the Cambrian to lower Silurian deep-water deposits of the Franklinian Basin and again as redeposited clasts in an upper Silurian conglomerate derived from uplifted and eroded Caledonian mountains in the northeast (Hopper and Ineson 2021, and references therein). However, the stratigraphic position of the meta-chert samples from the NBH dredge is unknown. The mid-Cretaceous age and special geochemical features of the mildly alkaline NBH basalts indicate a closer relationship of the northeastern YP to North America than to Svalbard at the time of magmatism.

Plate-tectonic implications for the southwestern Yermak Plateau: offshore continuation of Svalbard?

The SB alkaline basalts of the northern Sverdrup Bank with an age of 51 Ma do not have contemporaneous magmatic equivalents neither on Svalbard nor in the wider Arctic surroundings. At that time, the area of the future YP–Morris Jesup Rise was part of the continental margin of the young Eurasia Basin. In contrast to the mid-Cretaceous NBH mildly alkaline basalts, the early Eocene magmatism is not associated with significant high-amplitude positive magnetic anomalies. This implies that the Sverdrup Bank is not underlain by Cretaceous magmatic rocks and that this part of the future YP was originally located at greater distance from the area with the large positive magnetic anomalies. Thus, the southwestern YP was probably not directly connected with the Morris Jesup Rise and the northeastern YP, but was located closer to Svalbard.

The alkaline magmatism of the Sverdrup Bank was active during Stage 1 of the Eurekan deformation (53–47 Ma) that is characterized by compression along the west coast of Svalbard and the formation of the West Spitsbergen Fold-and-Thrust Belt (Piepjohn et al. 2016). However, the alkaline volcanism required an extensional tectonic environment. We speculate that the continental margin of the young Eurasia Basin between the area of the Morris Jesup Rise/northeastern YP (with the Cretaceous volcanic rocks) and offshore northwest Svalbard was affected by extension related to the formation of the Sophia Basin (Fig. 2a) and probably dextral strike-slip movements along deep-reaching faults, which gave rise to alkaline magmatism. Similar conditions were responsible for the volcanism of the Nares Strait alkaline suite at the sinistral Wegener Fault about 10 Ma earlier (Estrada et al. 2010).

Seismic refraction data from a NNW–SSE directed, 260 km long profile offshore along the northwestern Svalbard margin up to the southern end of the Sverdrup Bank (line AWI-99300; Fig. 2a) were interpreted as a northern continuation of the crustal structure of northwest Svalbard toward the YP and supposedly over the entire southwestern YP (Ritzmann and Jokat 2003). Sedimentary rocks of assumed late Silurian/Devonian age, possible equivalents of the Old Red Sandstone of northern Svalbard, form an older, up to 8 km thick, basin below the Oligocene Danskøya Basin (Fig. 2a) and represent the ca. 6 km thick upper section (below the Paleogene cover) north of the Danskøya Basin up to the northern end of the profile (Ritzmann and Jokat 2003).

The presence of partly reddish-colored sandstone samples in the SB dredge and in the SB-GC core recovered from the steep western slope of the northern Sverdrup Bank (Table 1) seems to support the interpretation of the seismic refraction data. In the SB-GBC core further east on the plateau, no sandstone was found (Fig. 2b). It is probably covered by the alkali basaltic lava.

The sandstone samples are petrographically very similar to sandstones of the Devonian Wood Bay Formation of the Andrée Land Group of Svalbard (Critelli and Reed 1999). The presence of plant fossils within the Devonian strata on Svalbard is described by Davies et al. (2021). However, the sandstone samples from the Sverdrup Bank are richer in carbonate than the typical Wood Bay sandstones. Together with the presence of limestones, this indicates shallow-water setting. Multi-colored sandstones and lithologically diverse limestones occur together within the Andrée Land Group (Dallmann 2015).

Red sandstones are infrequently present in dredges from the central part of Sverdrup Bank, which instead are dominated by pre-Devonian para- and orthogneisses as well as phyllites and schists (Kristoffersen et al. 2020). Two gneiss samples are also present in the SB dredge (Table 1). Such lithologies are known from northwest Svalbard. However, neither the metamorphic lithologies nor the sedimentary lithologies are exclusively present on northwest Svalbard. Without further analytical studies on the recovered sedimentary and metamorphic rock samples, the interpretation of the southwestern YP as a northern continuation of the basement of Svalbard remains speculative at this stage.

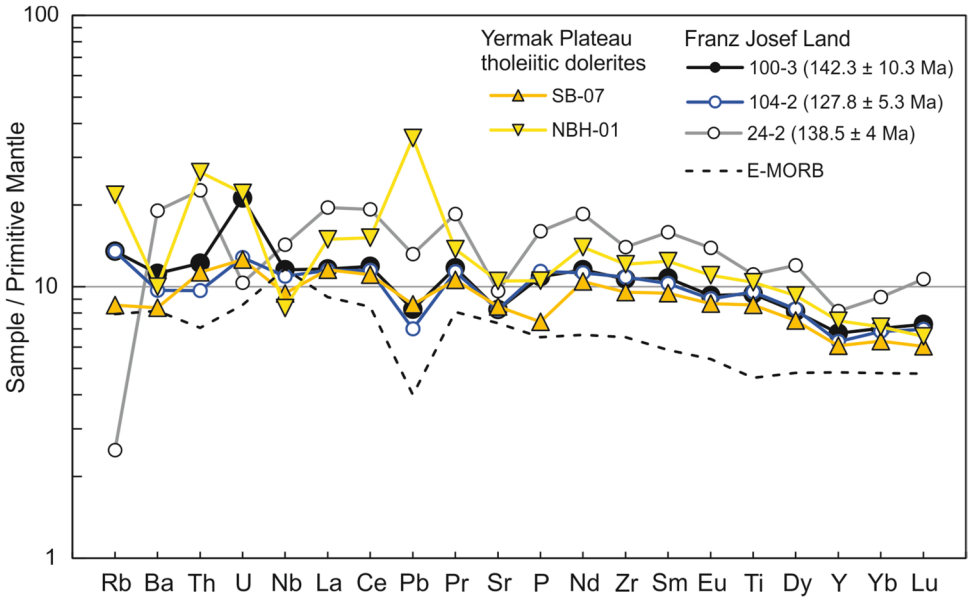

Fig. 11 Comparison of primitive-mantle (PM) normalized trace element concentrations of the Early Cretaceous tholeiitic dolerite samples from the NBH and SB dredges (data from Riefstahl et al. 2013) with coeval low-K tholeiitic basalt samples from Alexandra Land of Franz Josef Land (data from Karyakin et al. 2021). PM from McDonough and Sun (1995), E-MORB from Sun and McDonough (1989)

Origin of the dredged tholeiitic dolerite samples

The finding of HALIP-related volcanic rocks in the NBH dredge with ages of around 100 Ma begs the question of whether the two tholeiitic dolerite samples with Ar–Ar whole-rock ages of 133 ± 4 Ma (NBH dredge) and 144 ± 6 Ma (SB dredge) originate from intrusions into the YP basement during the first pulse of the HALIP magmatism, contrary to previous interpretations as ice-rafted debris (Riefstahl et al. 2013). The tholeiitic dolerite samples of the NBH and SB dredges coincide geochemically very well with the tholeiitic basalts from Franz Josef Land, as demonstrated by Riefstahl et al. (2013) using REE data from Ntaflos and Richter (2003). The Sr–Nd isotopic data of these samples also fit well to the field of the Franz Josef Land samples (Fig. 9). However, the Ar–Ar ages of the dredged tholeiitic basalts are somewhat older than the range of the first pulse of HALIP-related magmatism. Recently reported geochemical and Ar–Ar data show that the flood basalt magmatism on Franz Josef Land has a much longer age range with episodes from the Early Jurassic to the Early Cretaceous (Karyakin et al. 2021). Three samples from Alexandra Land, the westernmost island of the archipelago, with Ar–Ar plagioclase ages between ca. 142 and 128 Ma were selected from the dataset of Karyakin et al. (2021) to demonstrate the strong geochemical similarity with the coeval tholeiitic dredge samples (Fig. 11). In contrast, tholeiitic dolerites from Svalbard (Nejbert et al. 2011) are more evolved in the REE compared to the tholeiitic basalts from Franz Josef Land and from the tholeiitic dolerite samples of the NBH and SB dredge (Fig. 8B in Riefstahl et al. 2013). It should be mentioned that no tholeiitic sills or dykes of the first pulse of HALIP are known in northeast Ellesmere Island and North Greenland, which were, following our interpretation, adjacent to the northeastern YP during the middle Cretaceous. In summary, we follow the interpretation of Riefstahl et al. (2013) that the NBH and SB tholeiitic dolerite samples are most likely ice-transported from Franz Josef Land.

Comparison between HALIP-related alkaline and tholeiitic basalts and a link to the Alpha Ridge

Since we consider the mid-Cretaceous mildly alkaline NBH basalts as the cause for the strong positive magnetic anomalies of northeastern YP, we suggest that such magnetic anomalies over the conjugate Morris Jesup Rise (e.g., Jokat et al. 2016) are probably also caused by Cretaceous HALIP magmatic rocks. This anomaly pattern continues offshore toward northeastern Ellesmere Island and the Alpha Ridge (Jokat et al. 2016, and references therein). In the Yelverton Bay area at the north coast of Ellesmere Island, the magnetic pattern that covers the Alpha–Mendeleev Ridge overlaps with onshore areas (Fig. 1). There, the Hansen Point tholeiitic suite comprises felsic volcanic rocks with zircon U–Pb ages of 104–95 Ma (Estrada et al. 2016; Naber et al. 2021) and intrusions of basaltic dykes with Ar–Ar ages between ca. 97 and 83 Ma (Estrada and Henjes-Kunst 2013). The tholeiitic magmatism around Yelverton Bay was approximately coeval with the mildly alkaline volcanism of the Hassel Formation in the Lake Hazen area, the mildly alkaline volcanism of the northeastern YP, and the tholeiitic volcanism on the Alpha Ridge at ca. 89 Ma (sample PS051-041-1cc; see Fig. 1). Tholeiitic basalt samples dredged from the Chukchi Borderland (Fig. 1), which all were generated in a continental setting with thinning lithosphere, comprise low-Ti tholeiites with Ar–Ar ages of 118–112 Ma and

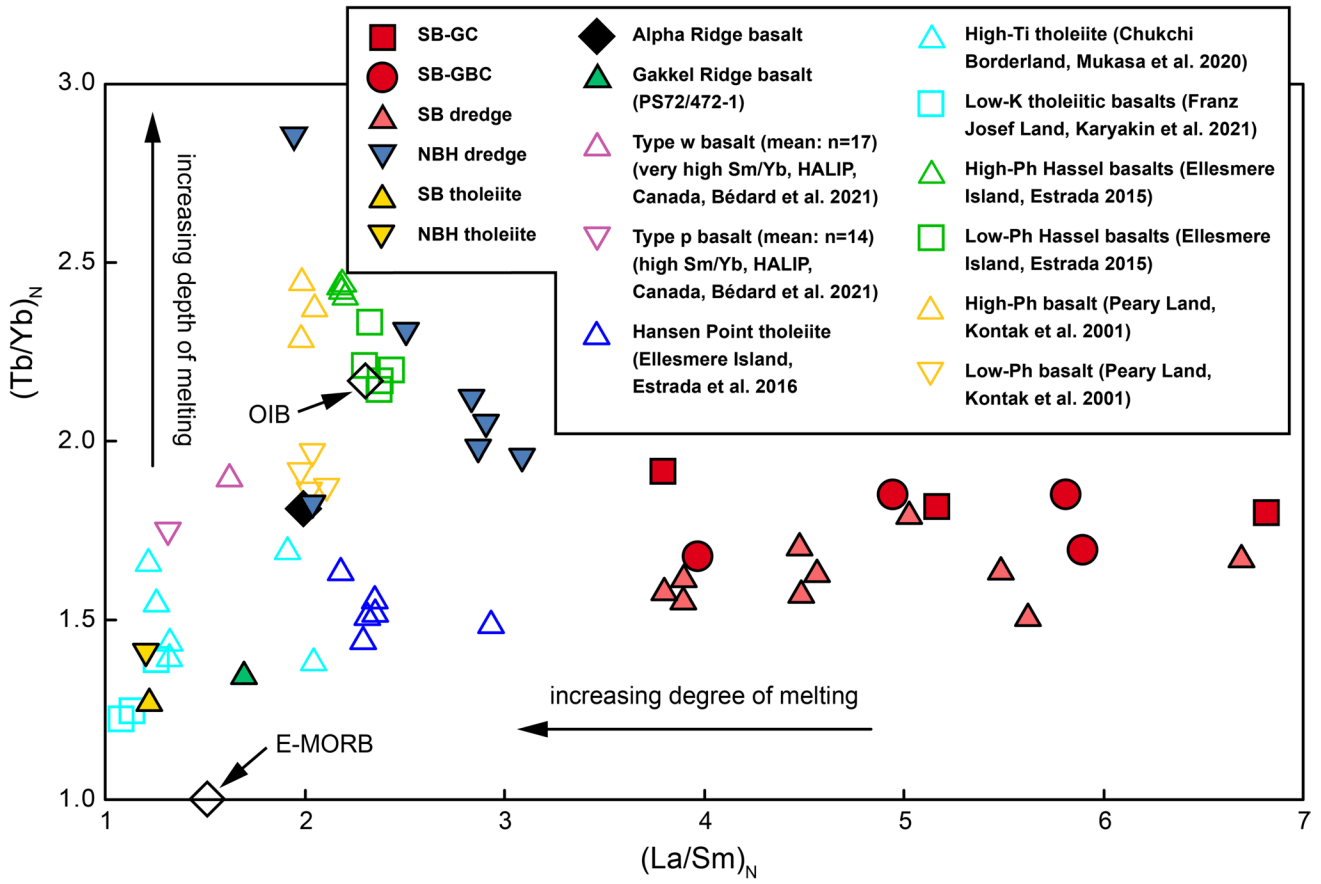

Fig. 12 Chondrite-normalized Tb/Yb vs. La/Sm diagram for the magmatic rocks from the YP compared with HALIP-related tholeiitic and alkaline magmatic rocks from the Canadian Arctic, North Greenland, Chukchi Borderland, Franz Josef Land, and Alpha Ridge. An alkaline basalt sample from the Siberian end of Gakkel Ridge (Jokat et al. 2019) is also shown. Chondrite, OIB, and E-MORB from Sun and McDonough (1989)

105–100 Ma as well as high-Ti tholeiites of ca. 90–70 Ma (Mukasa et al. 2020).

We compare all these HALIP-related tholeiitic and alkaline basalts in a diagram of chondrite-normalized ratios of Tb/Yb versus La/Sm that is indicative for the degree and depth of melting (Fig. 12). Most of the NBH samples are grouped close to OIB together with the high and low phosphorus basalts of the Hassel Formation from the Lake Hazen area and the slightly younger Peary Land dykes from North Greenland (see Fig. 10). The NBH samples have high $(Tb/Yb)_N$ values with a wide range indicating melt generation in several depths in the garnet-bearing mantle as well as in the transition zone between the garnet and spinel stability fields of the mantle.

The position of the high-phosphorus NBH-02 sample in the diagram (Fig. 12) is almost identical with that of the tholeiitic Alpha Ridge basalt sample indicating similar conditions for melt generation. Comparable high $(Tb/Yb)_N$ values are recorded in HALIP-related continental tholeiitic basalts of type w and type p from the Canadian Arctic (Bédard et al. 2021b). These tholeiite types show slightly lower $(La/Sm)_N$ values than the Alpha Ridge sample and thus were generated by larger degrees of melting. Samples of other tholeiitic suites, which plot partly close to the Alpha Ridge sample, belong to dykes of the Hansen Point tholeiitic suite and the high Ti basalts from Chukchi Borderland. The low-K tholeiite samples from Franz Josef Land and their ice-rafted equivalents from the YP dredges plot closer to E-MORB than the other tholeiites. They were generated by a high degree of melting beneath a strongly thinned continental crust. Even the most evolved alkaline basalt sample from the Siberian end of Gakkel Ridge (shown for comparison) plots closer to E-MORB than the Alpha Ridge sample. Due to the geochemical similarity of the Alpha Ridge basalt to continental tholeiitic basalts and transitional to mildly alkaline basalts from the surrounding Arctic regions, it can be concluded, that this basalt was generated in a continental environment. Probably, the Alpha–Mendeleev Ridge was partly or completely formed on a continental basement.

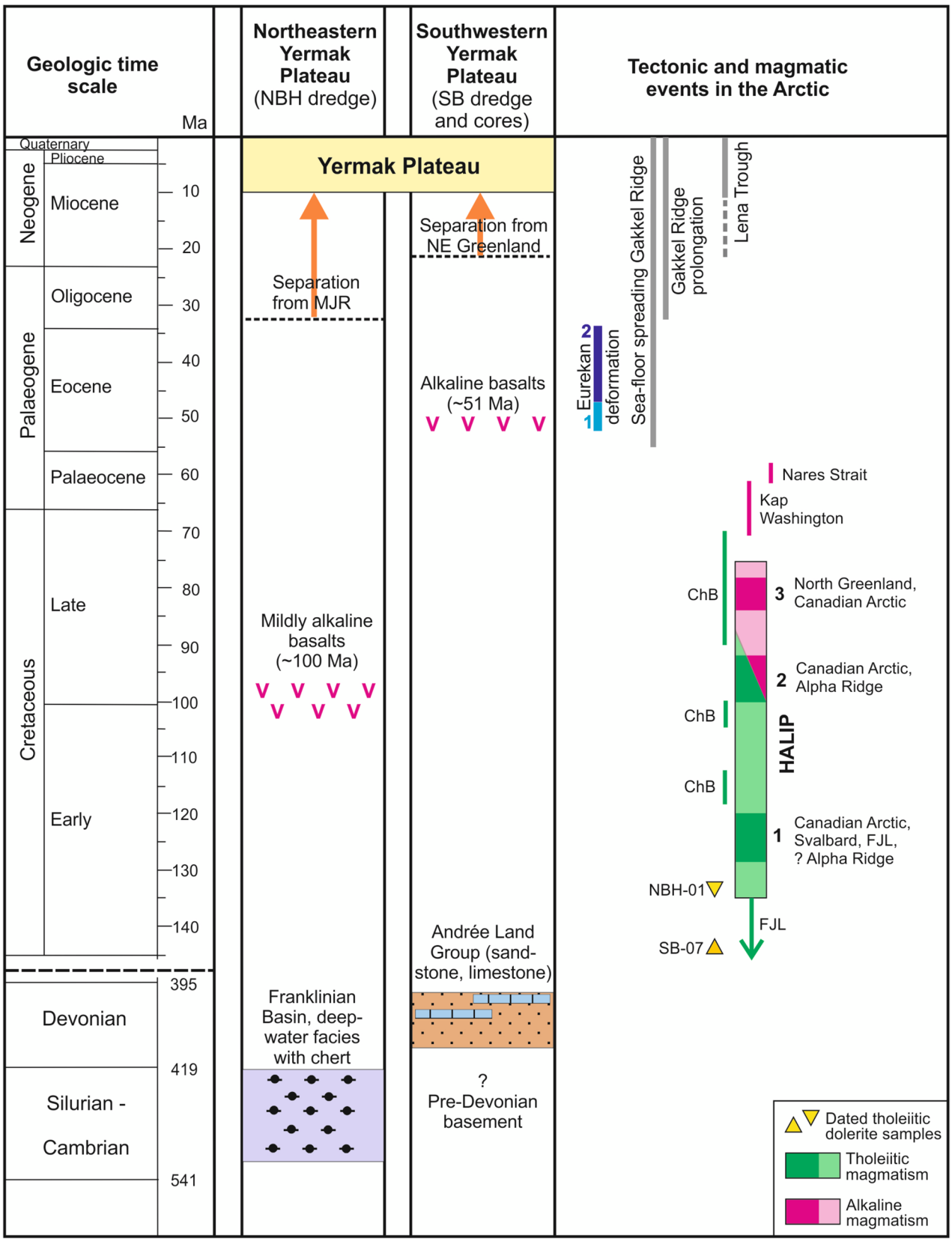
Geologic time scale
Ma
Quaternary
Pliocene
Neogene
Miocene
Palaeogene
Oligocene
Eocene
Palaeocene
Cretaceous
Late
Early
10
20
30
40
50
60
70
80
90
100
110
120
130
140
395
Devonian
419
Silurian -
Cambrian
541
Northeastern Yermak Plateau (NBH dredge)
Southwestern Yermak Plateau (SB dredge and cores)
Yermak Plateau
Separation from MJR
Separation from NE Greenland
Alkaline basalts (~51 Ma)
Mildly alkaline basalts (~100 Ma)
Franklinian Basin, deep-water facies with chert
Andrée Land Group (sand-stone, limestone)
? Pre-Devonian basement
Tectonic and magmatic events in the Arctic
Lena Trough
Gakkel Ridge prolongation
Sea-floor spreading Gakkel Ridge
Eurekan deformation
2
1
Nares Strait
Kap Washington
ChB
3
North Greenland, Canadian Arctic
2
Canadian Arctic, Alpha Ridge
ChB
HALIP
ChB
1
Canadian Arctic, Svalbard, FJL, ? Alpha Ridge
NBH-01
FJL
SB-07
Dated tholeiitic dolerite samples
Tholeiitic magmatism
Alkaline magmatism

◂**Fig. 13** Simplified stratigraphic chart showing the different composition and geologic development of the northeastern and southwestern YP interpreted from recovered basement rock samples. Cretaceous to recent tectonic and magmatic events in the Arctic are indicated for comparison (see text for references). Geologic time scale after Gradstein et al (2012). *ChB* Chukchi Borderland, *FJL* Franz Josef Land, *HALIP* High Arctic Large Igneous Province, *MJR* Morris Jesup Rise

The early Eocene alkali basalt samples from the Sverdrup Bank of the southwestern YP, were integrated into the diagram (Fig. 12) to again demonstrate their geochemical difference from the mildly alkaline NBH basalts from the northeastern YP. The high $(La/Sm)_N$ values with a wide range of the SB samples indicate magma generation from very small but different degrees of melting, whereas the relatively low and uniform $(Tb/Yb)_N$ values (mostly lower than those of the NBH samples) point to melting within the garnet-spinel stability transition zone or even of garnet-free mantle. However, petrogenetic studies of the magmatic rocks of the YP are beyond the scope of this study.

Conclusions

In this study, we present new data from rock fragments and sediments, which were cored from the Sverdrup Bank of the southwestern YP, together with a careful re-evaluation and new data of samples dredged from the southwestern YP (SB dredge) and northeastern YP (NBH dredge) published in Riefstahl et al. (2013). These combined data, compared with onshore and offshore volcanic and sedimentary rocks, reveal that the geological development of the northeastern YP and the southwestern YP is spatially and temporally different (Fig. 13).

1) The basaltic rocks from the northeastern YP are mildly alkaline with an estimated Ar–Ar age of ca. 100 Ma, which connects them to the second pulse of the HALIP-related alkaline and tholeiitic magmatism. Geochemically they resemble basaltic rocks of similar age of northeastern Ellesmere Island and North Greenland, which indicates a connection of these continental areas with the northeastern YP during the time of magmatism. Therefore, we suggest that the basement of the northeastern YP is a crustal fragment that was separated from North America due to the southward propagation of ocean-floor spreading along the Gakkel Ridge.
2) All alkaline basalt samples recovered from the northern Sverdrup Bank of the southwestern YP are petrographically and geochemically very similar and belong to a common volcanic suite. The volcanism was active at 51 Ma (Ar–Ar biotite ages; Riefstahl et al. 2013) in an extensional continental setting offshore northern Svalbard. The associated sedimentary rocks (reddish and gray sandstones, diverse limestones) resemble petrographically the Devonian Andrée Land Group ("Old Red Sandstone") of northern Svalbard; however, their stratigraphy or age is not determined.
3) We suppose that the high-amplitude magnetic anomalies of the northeastern YP and the conjugate Morris Jesup Rise are, at least partly, caused by the Cretaceous magmatism, which is evident in the NBH samples, and are not, or not only, associated with the propagation of the Gakkel Ridge toward North Greenland since ca. 33 Ma.
4) A tholeiitic basalt sample with an Ar–Ar age of ca. 89 Ma from the Alpha Ridge (Jokat et al. 2013) is geochemically well comparable with HALIP-related continental flood basalt samples and indicates a continental basement for parts of the Alpha–Mendeleev Ridge.
5) Single Early Cretaceous tholeiitic dolerite samples from both dredges are geochemically and geochronologically well comparable with rocks of Franz Josef Land, and are interpreted as ice-rafted debris.

Supplementary Information The online version contains supplementary material available at https://doi.org/10.1007/s00531-024-02389-8.

Acknowledgements Many thanks to Sebastian Flotow (laboratories of the Leibniz Centre for Tropical Marine Research, Bremen) for the preparation of the thin sections, to Yakov Kapusta (Actlabs, now at GeochronEx, Canada) for discussions on the $^{40}Ar/^{39}Ar$ dating results, to Friedhelm Henjes-Kunst (BGR, Hannover) for providing the Rb-Sr and Sm-Nd isotope data, to Kristian Ufer (BGR, Hannover) for the XRD data, and to Wilfried Jokat (AWI, Bremerhaven) for providing information and geochemical data of the Alpha Ridge sample PS051-041-1cc. Karsten Piepjohn (BGR, Hannover) is gratefully acknowledged for intense and fruitful discussion regarding structural development as well as support in the preparation of Fig. 3 and Rüdiger Lutz (BGR, Hannover) is greatly thanked for critical reading of an earlier version of the manuscript. We would like to express our great gratitude to Anna Sartell for critically reading, improving the English language, and helpful comments on the final version of the manuscript. We thank Editor-in-Chief Ulrich Riller, Jaroslaw Majka, and an anonymous reviewer for their constructive comments, which substantially improved the manuscript.

Author contributions All authors contributed to the study conception and design. The first draft of the manuscript was written by Solveig Estrada and Nikola Koglin. All authors commented on previous versions of the manuscript. All authors read and approved the final manuscript.

Funding Open Access funding enabled and organized by Projekt DEAL.

Data availability All data are available within this article and its supplementary material.

Declarations

Conflict of interest The authors have no conflicts of interest to declare that are relevant to the content of this article.

Open Access This article is licensed under a Creative Commons Attribution 4.0 International License, which permits use, sharing, adaptation, distribution and reproduction in any medium or format, as long as you give appropriate credit to the original author(s) and the source, provide a link to the Creative Commons licence, and indicate if changes were made. The images or other third party material in this article are included in the article's Creative Commons licence, unless indicated otherwise in a credit line to the material. If material is not included in the article's Creative Commons licence and your intended use is not permitted by statutory regulation or exceeds the permitted use, you will need to obtain permission directly from the copyright holder. To view a copy of this licence, visit http://creativecommons.org/licenses/by/4.0/.

References

Bédard JH, Troll VR, Deegan FM, Tegner C, Saumur BM, Evenchick CA, Grasby SE, Dewing K (2021a) High Arctic Large Igneous Province alkaline rocks in Canada: evidence for multiple mantle components. J Petrol 62:egab042. https://doi.org/10.1093/petrology/egab042

Bédard JH, Saumur BM, Tegner C, Troll VR, Deegan FM, Evenchick CA, Grasby SE, Dewing K (2021b) Geochemical systematics of High Arctic Large Igneous Province continental tholeiites from Canada—Evidence for progressive crustal contamination in the plumbing system. J Petrol 62:egab041. https://doi.org/10.1093/petrology/egab041

Beier C, Vanderkluysen L, Regelous M, Mahoney JJ, Garbe-Schönberg D (2011) Lithospheric control on geochemical composition along the Louisville Seamount Chain. Geochem Geophys Geosyst 12:Q0AM01. https://doi.org/10.1029/2011gc003690

Berglar K, Franke D, Lutz R, Schreckenberger B, Damm V (2016) Inital opening of the Eurasian Basin, Arctic Ocean. Front Earth Sci 4:91. https://doi.org/10.3389/feart.2016.00091

Brotzer A, Funck T, Geissler WH, Piepjohn K, Heyde I, Berglar K (2022) Geophysical insights on the crustal structure of Greenland's northern continental margin towards the Morris Jesup Spur. Tectonophysics 843:229588. https://doi.org/10.1016/j.tecto.2022.229588

Brozena JM, Childers VA, Lawver LA, Gahagan LM, Forsberg R, Faleide JI, Eldholm O (2003) New aerogeophysical study of the Eurasia Basin and Lomonosov Ridge: implications for basin development. Geology 31:825–828. https://doi.org/10.1130/G19528.1

Buchan KL, Ernst R (2006) Giant dyke swarms and the reconstruction of the Canadian Arctic islands, Greenland, Svalbard and Franz Josef Land. In: Mertanen S, Rämö T, Vuollo J (eds) Hanski E. Taylor & Francis, Dyke swarms—time markers of crustal evolution, pp 27–48

Buchan KL, Ernst RE (2018) A giant circumferential dyke swarm associated with the High Arctic Large Igneous Province (HALIP). Gondwana Res 58:39–57. https://doi.org/10.1016/j.gr.2018.02.006

Corfu F, Polteau S, Planke S, Faleide JI, Svensen H, Zayoncheck A, Stolbov N (2013) U–Pb geochronology of Cretaceous magmatism on Svalbard and Franz Josef Land, Barents Sea Large Igneous Province. Geol Mag 150:1127–1135. https://doi.org/10.1017/S0016756813000162

Crane K, Eldholm O, Myhre AM, Sundvor E (1982) Thermal implications for the evolution of the Spitsbergen transform fault. Tectonophysics 89:1–32. https://doi.org/10.1016/0040-1951(82)90032-4

Cressman ER (1962) Nondetrital siliceous sediments. In: Fleischer M (ed) Data of geochemistry, 6th edition, chapter T; Geological survey professional paper 440-T, Washington

Critelli S, Reed WE (1999) Provenance and stratigraphy of the Devonian (Old Red Sandstone) and Carboniferous sandstones of Spitsbergen, Svalbard. Eur J Mineral 11:149–166

Dallmann WK (2015) Geoscience atlas of Svalbard. Report series 148, Norsk Polarinstitutt, Oslo

Dallmann WK, Ohta Y, Elvevold S, Blomeier D (2002) Bedrock map of Svalbard and Jan Mayen, 1:750,000. Norsk Polarinstitutt Temakart 33, Tromsø

Davies NS, Berry CM, Marshall JEA, Wellman CH, Lindemann F-J (2021) The Devonian landscape factory: plant-sediment interaction in the Old Red Sandstone of Svalbard and the rise of vegetation as a biogeomorphic agent. J Geol Soc 178. https://doi.org/10.1144/jgs2020-225

Dowdeswell JA, Jakobsson M, Hogan KA, O'Regan M, Backman J, Evans J, Hell B, Löwemark L, Marcussen C, Noormets R, Cofaigh CÓ, Sellén E, Sölvsten M (2010) High-resolution geophysical observations of the Yermak Plateau and northern Svalbard margin: implications for ice-sheet grounding and deep-keeled icebergs. Quat Sci Rev 29:3518–3531. https://doi.org/10.1016/j.quascirev.2010.06.002

Drachev S, Saunders A (2006) The Early Cretaceous Arctic LIP: its geodynamic setting and implications for Canada Basin opening. In: Scott RA, Thurston DK (eds) Proceedings of the fourth International Conference on Arctic Margins, Anchorage, OCS study, MMS 2006-003, U.S. Department of the Interior, pp 216–223

Ehlers B-M, Jokat W (2013) Paleo-bathymetry of the northern North Atlantic and consequences for the opening of the Fram Strait. Mar Geophys Res 34:25–43. https://doi.org/10.1007/s11001-013-9165-9

Engen Ø, Faleide JI, Dyreng TK (2008) Opening of the Fram Strait gateway: a review of plate tectonic constraints. Tectonophysics 450:51–69. https://doi.org/10.1016/j.tecto.2008.01.002

Estrada S (2015) Geochemical and Sr–Nd isotope variations within Cretaceous continental flood-basalt suites of the Canadian High Arctic, with a focus on the Hassel Formations basalts of northeast Ellesmere Island. Int J Earth Sci 104:1981–2005. https://doi.org/10.1007/s00531-014-1066-x

Estrada S, Henjes-Kunst F (2004) Volcanism in the Canadian High Arctic related to the opening of the Arctic Ocean. Zeitschrift der Dtsch Geol Gesellschaft 154:579–603. https://doi.org/10.1127/zdgg/154/2004/579

Estrada S, Henjes-Kunst F (2013) ^{40}Ar–^{39}Ar and U–Pb dating of Cretaceous continental rift-related magmatism on the northeast Canadian Arctic margin. Zeitschrift der Deutschen Gesellschaft für Geowissenschaften (German J Geosci) 164:107–130. https://doi.org/10.1127/1860-1804/2013/0005

Estrada S, Höhndorf A, Henjes-Kunst F (2001) Cretaceous/tertiary volcanism in North Greenland: the Kap Washington Group. Polarforschung 69:17–23. https://doi.org/10.2312/polarforschung.69.17

Estrada S, Henjes-Kunst F, Melcher F, Tessensohn F (2010) Paleocene alkaline volcanism in the Nares Strait region: evidence from volcanic pebbles. Int J Earth Sci 99:863–890. https://doi.org/10.1007/s00531-009-0432-6

Estrada S, Damaske D, Henjes-Kunst F, Schreckenberger B, Oakey GN, Piepjohn K, Eckelmann K, Linnemann U (2016) Multistage Cretaceous magmatism in the northern coastal region of Ellesmere Island and its relation to the formation of Alpha Ridge—evidence from aeromagnetic, geochemical and geochronological data. Nor J Geol 96:65–95. https://doi.org/10.17850/njg96-2-03

Feden RH, Vogt PR, Fleming HS (1979) Magnetic and bathymetric evidence for the "Yermak hot spot" northwest of Svalbard in the Arctic Basin. Earth Planet Sci Lett 44:18–38. https://doi.org/10.1016/0012-821X(79)90004-9

Gaina C, Gernigon I, Ball P (2009) Palaeocene—recent plate boundaries in the NE Atlantic and the formation of the Jan Mayen microcontinent. J Geol Soc Lond 166:601–616. https://doi.org/10.1144/0016-76492008-112

Gaina C, Nasuti A, Kimbell GS, Blischke A (2017) Break-up and seafloor spreading domains in the NE Atlantic. In: Péron-Pinvidic G, Hopper JR, Stoker MS, Gaina C, Doornenbal JC, Funck T, Árting UE (eds) The NE Atlantic region: a reappraisal of crustal structure, tectonostratigraphy and magmatic evolution, vol 447. Special publications. Geological Society, London, pp 393–417. https://doi.org/10.1144/SP447.12

Gebhardt AC, Jokat W, Niessen F, Matthiessen J, Geissler WH, Schenke HW (2011) Ice sheet grounding and iceberg plow marks on the northern and central Yermak Plateau revealed by geophysical data. Quat Sci Rev 30:1726–1738. https://doi.org/10.1016/j.quascirev.2011.03.016

Geissler WH, Jokat W (2004) A geophysical study of the northern Svalbard continental margin. Geophys J Int 158:50–66. https://doi.org/10.1111/j.1365-246X.2004.02315.x

Geissler WH, Jokat W, Brekke H (2011) The Yermak Plateau in the Arctic Ocean in the light of reflection seismic data—implication for its tectonic and sedimentary evolution. Geophys J Int 187:1334–1362. https://doi.org/10.1111/j.1365-246X.2011.05197.x

Geissler WH, Estrada S, Riefstahl F, O'Connor JM, Spiegel C, Van den Boogard P, Klügel A (2019) Middle Miocene magmatic activity in the Sophia Basin, Arctic Ocean—evidence from dredged basalt at the flanks of Mosby Seamount. Arktos 5:31–48. https://doi.org/10.1007/s41063-019-00066-8

Gerlings J, Funck T, Jackson HR, Louden KE, Klingelhofer F (2009) Seismic evidence for plume-derived volcanism during formation of the continental margin in southern Davis Strait and northern Labrador Sea. Geophys J Int 176:980–994. https://doi.org/10.1111/j.1365-246X.2008.04021.x

Gernigon L, Gaina C, Olesen O, Ball PJ, Péron-Pinvidic G, Yamasaki T (2012) The Norway Basin revisited: from continental breakup to spreading ridge extinction. Mar Pet Geol 35:1–19. https://doi.org/10.1016/j.marpetgeo.2012.02.015

Gernigon L, Franke D, Geoffroy L, Schiffer C, Foulger GR, Stoker M (2020) Crustal fragmentation, magmatism, and the diachronous opening of the Norwegian-Greenland Sea. Earth Sci Rev 206:102839. https://doi.org/10.1016/j.earscirev.2019.04.011

Glebovsky VYu, Kaminsky VD, Minakov AN, Merkur'ev SA, Childers VA, Brozena JM (2006) Formation of the Eurasia Basin in the Arctic Ocean as inferred from geohistorical analysis of the anomalous magnetic field. Geotectonics 40:263–281

Gradstein FM, Ogg JG, Hilgen FJ (2012) On the Geologic Time Scale. Newsl Stratigr 45:171–188. https://doi.org/10.1127/0078-0421/2012/0020

Hofmann AW (2003) Sampling mantle heterogeneity through oceanic basalts: isotopes and trace elements. In: Holland HD, Turekian KK (eds) Treatise on Geochemistry, vol 2. Elsevier, Amsterdam, pp 1–44. https://doi.org/10.1016/B0-08-043751-6/02123-X

Hopper JR, Ineson JR (2021) Franklinian Composite Tectono-Sedimentary Element, North Greenland. In: Drachev SS, Brekke H, Henriksen E, Moore T (eds) Sedimentary successions of the Arctic region and their hydrocarbon prospectivity. Memoirs 57. Geological Society, London. https://doi.org/10.1144/M57-2020-6

Jackson HR, Johnson GL, Sundvor E, Myhre AM (1984) The Yermak Plateau: formed at a triple junction. J Geophys Res 89(B5):3223–3232. https://doi.org/10.1029/JB089iB05p03223

Jakobsson M, Backman J, Rudels B, Nycander J, Frank M, Mayer L, Jokat W, Sangiorgi F, O'Regan M, Brinkhuis H, King J, Moran K (2007) The early Miocene onset of a ventilated circulation regime in the Arctic Ocean. Nature 447:986–990. https://doi.org/10.1038/nature05924

Jakobsson M, Nilsson J, O'Regan M, Backman J, Löwemark L, Dowdeswell JA, Mayer L, Polyak L, Colleoni F, Anderson LG, Björk G, Darby D, Eriksson B, Hanslik D, Hell B, Marcussen C, Sellén E, Wallin Å (2010) An Arctic Ocean ice shelf during MIS 6 constrained by new geophysical and geological data. Quat Sci Rev 29:3505–3517. https://doi.org/10.1016/j.quascirev.2010.03.015

Jakobsson M, Andreassen K, Bjarnadóttir LR, Dove D, Dowdeswell JA, England JH, Funder S, Hogan K, Ingólfsson Ó, Jennings A, Larsen NK, Kirchner N, Landvik JY, Mayer L, Mikkelsen N, Möller P, Niessen F, Nilsson J, O'Regan M, Polyak L, Nørgaard-Pedersen N, Stein R (2014) Arctic Ocean glacial history. Quat Sci Rev 92:40–67. https://doi.org/10.1016/j.quascirev.2013.07.033

Jakobsson M, Mayer LA, Bringensparr C, Castro CF, Mohammad R, Johnson P, Ketter T et al (2020) The International Bathymetric Chart of the Arctic Ocean Version 4.0. Sci Data 7:176. https://doi.org/10.1038/s41597-020-0520-9

Jokat W (1999) Arctic '98: The expedition ARK-XIV/l a of RV "Polarstern" in 1998. Ber Polarforsch 308:1–159. https://doi.org/10.2312/BzP_0308_1999

Jokat W, Weigelt E, Kristoffersen Y, Rasmussen T, Schöne T (1995) New geophysical results from the south-western Eurasian Basin (Morris Jesup Rise, Gakkel Ridge, Yermak Plateau) and the Fram Strait. Geophys J Int 123:601–610. https://doi.org/10.1111/j.1365-246X.1995.tb06874.x

Jokat W, Stein R, Rachor E, Schewe I et al (1999) Expedition gives fresh view of central Arctic geology. Eos Trans AGU 80(40):465–480. https://doi.org/10.1029/EO080i040p00465-01

Jokat W, Geissler W, Voss M (2008) Basement structure of the northwestern Yermak Plateau. Geophys Res Lett 35:L05309. https://doi.org/10.1029/2007GL032892

Jokat W, Ickrath M, O'Connor J (2013) Seismic transect across the Lomonosov and Mendeleev Ridges: constraints on the geological evolution of the Amerasia Basin, Arctic Ocean. Geophys Res Lett 40:5047–5051. https://doi.org/10.1002/grl.50975

Jokat W, Lehmann P, Damaske D, Nelson JB (2016) Magnetic signature of North-East Greenland, the Morris Jesup Rise, the Yermak Plateau, the central Fram Strait: constraints for the rift/drift history between Greenland and Svalbard since the Eocene. Tectonophysics 691:98–109. https://doi.org/10.1016/j.tecto.2015.12.002

Jokat W, O'Connor J, Hauff F, Koppers AAP, Miggins DP (2019) Ultraslow spreading and volcanism at the eastern end of Gakkel Ridge, Arctic Ocean. Geochem Geophys Geosyst 20:6033–6050. https://doi.org/10.1029/2019GC008297

Karyakin YuV, Aleksandrova GN (2022) Early Jurassic flood basalt volcanism on Franz Josef Land Archipelago: geological and palynostratigraphical data. Stratigr Geol Correl 30(Suppl. 1):S23–S46. https://doi.org/10.1134/S0869593823010033

Karyakin YuV, Sklyarov EV, Travin AV (2021) Plume magmatism at Franz Josef Land. Petrology 29:528–560. https://doi.org/10.1134/S0869591121050027

Kleinspehn KL, Teyssier C (2016) Oblique rifting and the Late Eocene-Oligocene demise of Laurasia with inception of Molloy Ridge: deformation of Forlandsundet Basin, Svalbard. Tectonophysics 693:363–377. https://doi.org/10.1016/j.tecto.2016.05.010

Kontak DJ, Jensen SM, Dostal J, Archibald DA, Kyser TK (2001) Cretaceous mafic dyke swarm, Peary Land, northernmost Greenland: geochronolgy and petrology. Can Mineral 39:997–1020. https://doi.org/10.2113/gscanmin.39.4.997

Kristoffersen Y, Talwani M (1977) Extinct triple junction south of Greenland and the Tertiary motion of Greenland relative to North

America. Geol Soc Am Bull 88:1037–1049. https://doi.org/10.1130/0016-7606(1977)88%3c1037:ETJSOG%3e2.0.CO;2
Kristoffersen Y, Hall JK (2014) Hovercraft as a mobile science platform over sea ice in the Arctic Ocean. Oceanography 27:170–179. https://doi.org/10.5670/oceanog.2014.33
Kristoffersen Y, Ohta Y, Hall JK (2020) On the the origin of the Yermak Plateau north of Svalbard, Arctic Ocean. Nor J Geol 100:202006. https://doi.org/10.17850/njg100-1-5
Lutz R, Franke D, Berglar K, Heyde I, Schreckenberger B, Klitzke P, Geissler WH (2018) Evidence for mantle exhumation since the early evolution of the slow-spreading Gakkel Ridge, Arctic Ocean. J Geodyn 118:154–165. https://doi.org/10.1016/j.jog.2018.01.014
McDonough WF, Sun S-S (1995) The composition of the Earth. Chem Geol 120:223–253. https://doi.org/10.1016/0009-2541(94)00140-4
Meschede M (1986) A method of discriminating between different types of mid-ocean ridge basalts and continental tholeiites with the Nb–Zr–Y diagram. Chem Geol 56:207–218. https://doi.org/10.1016/0009-2541(86)90004-5
Mühe R, Jokat W (2004) First igneous rocks from the Alpha Ridge, Arctic Ocean: petrography and geochemistry. Unpublished manuscript, Library archive of Federal Institute for Geosciences and Natural Resources (BGR), Hannover, Germany, catalogue number OASYS 208078
Mukasa SB, Andronikov A, Brumley K, Mayer LA, Armstrong A (2020) Basalts from the Chukchi borderland: ^{40}Ar/^{39}Ar ages and geochemistry of submarine intraplate lavas dredged from the western Arctic Ocean. J Geophys Res Solid Earth 125:e2019JB017604. https://doi.org/10.1029/2019JB017604
Naber TV, Grasby SE, Cuthbertson JP, Rayner N, Tegner C (2021) New constraints on the age, geochemistry, and environmental impact of High Arctic Large Igneous Province magmatism: tracing the extension of the Alpha Ridge onto Ellesmere Island, Canada. GSA Bull 133:1695–1711. https://doi.org/10.1130/b35792.1
Nejbert K, Krajewski KP, Dubińska E, Pécskay Z (2011) Dolerites of Svalbard, northwest Barents Sea Shelf: age, tectonic setting and significance for geotectonic interpretation of the High-Arctic Large Igneous Province. Polar Res 30:7306. https://doi.org/10.3402/polar.v30i0.7306
Ntaflos T, Richter W (2003) Geochemical constraints on the origin of the Continental Flood Basalt magmatism in Franz Josef Land, Arctic Russia. Eur J Mineral 15:649–663. https://doi.org/10.1127/0935-1221/2003/0015-0649
Oakey GN, Saltus RW (2016) Geophysical analysis of the Alapha-Mendeleev ridge complex: characterization of the High Arctic Large Igeneous Province. Tectonophysics 691:65–84. https://doi.org/10.1016/j.tecto.2016.08.005
Okay N, Crane K (1993) Thermal rejuvenation of the Yermak Plateau. Mar Geophys Res 15:243–263. https://doi.org/10.1007/BF01982384
Osadetz KG, Moore PR (1988) Basic volcanics in the Hassel Formation (mid-Cretaceous) and associated intrusives, Ellesmere Island, District of Franklin, Northwest Territories. Paper 87–21, Geological Survey of Canada, Ottawa
Pearce JA (1996) A user's guide to basalt discrimination diagrams. In: Wyman DA (ed) Trace element geochemistry of volcanic rocks: applications for massive sulphide exploration. Geological Association of Canada, Short Course Notes, vol 12, pp 79–113
Pearce JA (2008) Geochemical fingerprinting of oceanic basalts with applications to ophiolite classification and the search for Archean oceanic crust. Lithos 100:14–48. https://doi.org/10.1016/j.lithos.2007.06.016
Phillips RL, Grantz A (2001) Regional variations in provenance and abundance of icerafted clasts in Arctic Ocean sediments: implications for the configuration of late Quaternary oceanic and atmospheric circulation in the Arctic. Mar Geol 172:91–115
Piepjohn K, von Gosen W, Tessensohn F (2016) The Eurekan deformation in the Arctic: an outline. J Geol Soc 173:1007–1024. https://doi.org/10.1144/jgs2016-081
Polteau S, Hendriks BWH, Planke S, Ganerød M, Corfu F, Faleide JI, Midtkandal I, Svensen HS, Myklebust R (2016) The Early Cretaceous Barents Sea Sill Complex: distribution, ^{40}Ar/^{39}Ar geochronology, and implications for carbon gas formation. Palaeogeogr Palaeoclimatol Palaeoecol 441:83–95. https://doi.org/10.1016/j.palaeo.2015.07.007
Riefstahl F, Estrada S, Geissler WH, Jokat W, Stein R, Kämpf H, Dulski P, Naumann R, Spiegel C (2013) Provenance and characteristics of rocks from the Yermak Plateau, Arctic Ocean: petrographic, geochemical and geochronological constraints. Mar Geol 343:125–145. https://doi.org/10.1016/j.margeo.2013.06.009
Ritzmann O, Jokat W (2003) Crustal structure of northwestern Svalbard and the adjacent Yermak Plateau: evidence for Oligocene detachment tectonics and non-volcanic breakup. Geophys J Int 152:139–159. https://doi.org/10.1046/j.1365-246X.2003.01836.x
Saltus RW, Miller EL, Gaina C, Brown PJ (2011) Regional magnetic domains of the Circum-Arctic: a framework for geodynamic interpretation. In: Spencer AM, Embry AF, Gautier DL, Stoupakova AV, Sørensen K (eds) Arctic petroleum geology. Memoirs 35. The Geological Society of London, London, pp 49–60. https://doi.org/10.1144/M35.4
Schiffer C, Stephenson R (2017) Regional crustal architecture of Ellesmere Island, Arctic Canada. In: Pease V, Coakley B (eds) Circum-arctic lithosphere evolution, vol 460. Special publications. Geological Society, London. https://doi.org/10.1144/SP460.8
Schiffer C, Stephenson R, Oakey GN, Jacobsen BH (2016) The crustal structure of Ellesmere Island, Arctic Canada—teleseismic mapping across a remote intraplate orogenic belt. Geophys J Int 204:1579–1600. https://doi.org/10.1093/gji/ggv539
Schneider DA, Faehnrich K, Majka J, Manecki M (2019) ^{40}Ar/ ^{39}Ar geochronologic evidence of Eurekan deformation within the West Spitsbergen Fold and Thrust Belt. In: Piepjohn K, Strauss VJ, Reinhardt L, McClelland WC (eds) Circum-Arctic structural events: tectonic evolution of the Arctic margins and trans-Arctic links with adjacent orogens, vol 541. Special paper. Geological Society of America, Boulder, pp 153–168. https://doi.org/10.1130/2018.2541(08)
Senger K, Galland O (2022) Stratigraphic and spatial extent of HALIP magmatism in central Spitsbergen. Geochem Geophys Geosyst 23:e2021GC010300. https://doi.org/10.1029/2021GC010300
Senger K, Tveranger J, Ogata K, Braathen A, Planke S (2014) Late Mesozoic magmatism in Svalbard: a review. Earth-Science Rev 139:123–144. https://doi.org/10.1016/j.earscirev.2014.09.002
Shervais JW (1982) Ti-V plots and the petrogenesis of modern and ophiolitic lavas. Earth Planet Sci Lett 59:101–118. https://doi.org/10.1016/0012-821X(82)90120-0
Shipilov EV (2015) Late Mesozoic magmatism and Cenozoic tectonic deformations of the Barents Sea continental margin: effect on hydrocarbon potential distribution. Geotectonics 49:53–74. https://doi.org/10.1134/S0016852115010045
Shipilov EV, Karyakin YV (2011) The Barents Sea magmatic province: geological-geophysical evidence and new ^{40}Ar/^{39}Ar dates. Dokl Earth Sci 439:955–960. https://doi.org/10.1134/S1028334X11070270
Snow JE, Hellebrand E, von der Handt A, Nauret F, Gao Y, Schenke HW (2011) Oblique nonvolcanic seafloor spreading in Lena Trough. Arctic Ocean Geochem Geophys Geosyst 12:Q10009. https://doi.org/10.1029/2011GC003768
Spielhagen RF, Baumann KH, Erlenkeuser H, Nowaczyk NR, Nørgaard-Pedersen N, Vogt C, Weiel D (2004) Arctic Ocean

deep-sea record of northern Eurasian ice sheet history. Quat Sci Rev 23:1455–1483. https://doi.org/10.1016/j.quascirev.2003.12.015

Srivastava SP (1978) Evolution of the Labrador Sea and its bearing on the early evolution of the North Atlantic. Geophys J R Astron Soc 52:313–357. https://doi.org/10.1111/j.1365-246X.1978.tb04235.x

Srivastava SP, Tapscott CR (1986) Plate kinematics of the North Atlantic. In: Vogt PR, Tucholke BE (eds) The geology of North America, vol M the Northern West Atlantic region. Geological Society of America, Boulder, pp 379–405

Staudigel H, Plank T, White WM, Schmincke HU (1996) Geochemical fluxus during seafloor alteration of the basaltic upper crust: DSDP sites 417 and 418. In: Bebout GE, Scholl DW, Kirby SH, Platt JP (eds) Subduction: top to bottom. Geophys Monogr Ser. AGU, Washington D.C, pp 19–38

Stein R (ed) (2005) Scientific cruise report of the Arctic Expedition ARK-XX/3 of RV Polarstern in 2004: Fram Strait, Yermak Plateau and East Greenland continental margin. Reports Polar Mar. Res. 517, Alfred Wegener Institute for Polar and Marine Research, Bremerhaven, Germany, p 188. https://doi.org/10.2312/BzPM_0517_2005

Stephenson R, Piepjohn K, Schiffer C, von Gosen W, Oakey GN, Anudu G (2017) Integrated crustal-geological cross-section of Ellesmere Island. In: Pease V, Coakley B (eds) Circum-Arctic lithosphere evolution, vol 460. Special publications. Geological Society, London. https://doi.org/10.1144/SP460.12

Storey M, Duncan RA, Pedersen AK, Larsen LM, Larsen HC (1998) $^{40}Ar/^{39}Ar$ geochronology of the West Greenland Tertiary volcanic province. Earth Planet Sci Lett 160:569–586. https://doi.org/10.1016/S0012-821X(98)00112-5

Storey M, Duncan RA, Tegner C (2007) Timing and duration of volcanism in the North Atlantic Igneous Province: implications for geodynamics and links to the Iceland hotspot. Chem Geol 241:264–281. https://doi.org/10.1016/j.chemgeo.2007.01.016

Strand K, Junttila J, Lahtinen T, Turunen S (2008) Climatic transition in the Arctic as revealed by mineralogical evidence from the Upper Cenozoic sediments in the central Arctic Ocean and the Yermak Plateau. Norw J Geol 88:305–312

Sun S-s, McDonough WF (1989) Chemical and isotopic systematics of oceanic basalts: implications for mantle composition and processes. Geol Soc Lond Spec Publ 42:313–345. https://doi.org/10.1144/GSL.SP.1989.042.01.19

Svendsen JI, Alexanderson H, Astakhov VI, Demidov I, Dowdeswell JA, Funder S, Gataullin V, Henriksen M, Hjort C, Houmark-Nielsen M, Hubberten HW, Ingólfsson Ó, Jakobsson M, Kjær KH, Larsen E, Lokrantz H, Lunkka JP, Lyså A, Mangerud J, Matiouchkov A, Murray A, Möller P, Niessen F, Nikolskaya O, Polyak L, Saarnisto M, Siegert C, Siegert MJ, Spielhagen RF, Stein R (2004) Late Quaternary ice sheet history of northern Eurasia. Quat Sci Rev 23:1229–1271. https://doi.org/10.1016/j.quascirev.2003.12.008

Talwani M, Eldholm O (1977) Evolution of the Norwegian-Greenland Sea. Geol Soc Am Bull 88:969–999. https://doi.org/10.1130/0016-7606(1977)88%3c969:EOTNS%3e2.0.CO;2

Tegner C, Brooks CK, Duncan RA, Heister LE, Bernstein S (2008) $^{40}Ar–^{39}Ar$ ages of intrusions in East Greenland: Rift-to-drift transition over the Iceland hotspot. Lithos 101:480–500. https://doi.org/10.1016/j.lithos.2007.09.001

Tegner C, Storey M, Holm PM, Thórarinsson SB, Zhao X, Lo CH, Knudsen MF (2011) Magmatism and Eurekan deformation in the High Arctic Large Igneous Province: $^{40}Ar–^{39}Ar$ age of Kap Washington Group volcanics, North Greenland. Earth Planet Sci Lett 303:203–214. https://doi.org/10.1016/j.epsl.2010.12.047

Tessensohn F, Piepjohn K (2000) Eocene compressive deformation in Arctic Canada, North Greenland and Svalbard and its plate tectonic causes. Polarforschung 68:121–124. https://doi.org/10.2312/polarforschung.68.121

Thórarinsson SB, Holm PM, Tappe S, Heaman LM, Tegner C (2011) Late Cretaceous-Palaeocene continental rifting in the High Arctic: U–Pb geochronology of the Kap Washington Group volcanic sequence, North Greenland. J Geol Soc Lond 168:1093–1106. https://doi.org/10.1144/0016-76492011-018

Thórarinsson SB, Söderlund U, Døssing A, Holm PM, Ernst RE, Tegner C (2015) Rift magmatism on the Eurasia basin margin: U–Pb baddeleyite ages of alkaline dyke swarms in North Greenland. J Geol Soc 172:721–726. https://doi.org/10.1144/jgs2015-049

Van Wagoner NA, Robinson PT (1985) Petrology and geochemistry of a CESAR bedrock sample: implications for the origin of the Alpha Ridge. In: Jackson HR, Mudie PJ, Blasco SM (eds) Initial geological report on CESAR—the Canadian expedition to study the Alpha Ridge, Arctic Ocean, Geological Survey of Canada paper 84–22, pp 47–57

Van Wagoner NA, Williamson M-C, Robinson PT, Gibson IL (1986) First samples of acoustic basement recovered from the Alpha Ridge, Arctic Ocean: new constraints for the origin of the ridge. J Geodyn 6:177–196

Vogt PR, Taylor PT, Kovacs LC, Johnson GL (1979) Detailed aeromagnetic investigation of the Arctic Basin. J Geophys Res 84(B3):1071–1089. https://doi.org/10.1029/JB084iB03p01071

Vogt PR, Crane K, Sundvor E (1994) Deep Pleistocene iceberg plowmarks on the Yermak Plateau: sidescan and 3.5 kHz evidence for thick claving ice fronts and a possible marine ice sheet in the Arctic Ocean. Geology 22:403–406

Wang J, Chen D, Wang D, Yan D, Zhou X, Wang Q (2012) Petrology and geochemistry of chert on the marginal zone of Yangtze Platform, western Hunan, South China, during the Ediacaran-Cambrian transition. Sedimentology 59:809–829. https://doi.org/10.1111/j.1365-3091.2011.01280.x

Whitney DL, Evans BW (2010) Abbreviations for names of rock-forming minerals. Am Miner 95:185–187. https://doi.org/10.2138/am.2010.3371

Williamson M-C, Kellet D, Miggins D, Koppers A, Carey R, Oakey G, Weis D, Jokat W, Massey E (2019) Age and eruptive style of volcanic rocks dredged from the Alpha Ridge, Arctic Ocean. Geophys Res Abstr, 21: EGU2019-6336. https://meetingorganizer.copernicus.org/EGU2019/EGU2019-6336.pdf

Winchester JA, Floyd PA (1977) Geochemical discrimination of different magma series and their differentiation products using immobile elements. Chem Geol 20:325–343. https://doi.org/10.1016/0009-2541(77)90057-2